Inorganic Chemistry

Article

pubs.acs.org/IC

Effects of Sequence, Connectivity, and Counter Ions in New Amide-Linked Ru(tpy)$_2$–Re(bpy) Chromophores on Redox Chemistry and Photophysics

Jan Dietrich, Ute Thorenz, Christoph Förster, and Katja Heinze*

Institute of Inorganic Chemistry and Analytical Chemistry, Johannes Gutenberg—University of Mainz, Duesbergweg 10-14, 55128 Mainz, Germany

Supporting Information

ABSTRACT: New cationic metallo ligands **L1**–**L3** based on bis(terpyridine) ruthenium(II) complexes decorated with differently substituted 2,2′-bipyridines attached via amide groups (5-NHCO-bpy, 4-CONH-bpy, 5-CONH-bpy) were prepared. Coordination of $Re^{I}Cl(CO)_3$ fragments to the bpy unit gives the corresponding bimetallic Ru∼Re complexes **1**–**3**. Hydrogen bonds of the bridging amide groups to $[PF_6]^-$ counterions or to water molecules are observed both in the solid state and in solution. The impact of the amide orientation, the connecting site, and the coordination of counterions on redox and photophysical properties is explored. Both the metallo ligands **L1**–**L3** and the bimetallic complexes **1**–**3** are emissive at room temperature in fluid solution. The emission originates from ^{3}MLCT(Ru) states in all cases. Accordingly, the first oxidation of **L1**–**L3** and **1**–**3** to $[\mathbf{L1}]^+$–$[\mathbf{L3}]^+$ and $[\mathbf{1}]^+$–$[\mathbf{3}]^+$ is assigned to the $Ru^{II/III}$ couple, while the first reduction to $[\mathbf{L1}]^-$–$[\mathbf{L3}]^-$ and $[\mathbf{1}]^-$–$[\mathbf{3}]^-$ occurs at the tpy-CO ligand as shown by UV/vis, IR, and EPR spectroscopy of the chemically generated radicals. Under rapid freezing conditions, radicals $[\mathbf{2}]^-$ and $[\mathbf{3}]^-$ are stabilized as different valence isomers with the odd electron localized at the $[\text{bpy-CO}]^\bullet$ bridging unit instead of the $[\text{tpy-CO}]^\bullet$. Furthermore, in radical $[\mathbf{3}]^-$ this valence equilibrium is shifted from $[\text{bpy-CO}]^\bullet$ to $[\text{tpy-CO}]^\bullet$ by coordination of $[PF_6]^-$ counterions to the bridging amide unit and back by replacing the $[PF_6]^-$ counterion with $[BPh_4]^-$. Photoinduced electron transfer (λ_{exc} = 500 nm) to **L1**–**L3** and to **1**–**3** is successful using triethanolamine (TEOA) as a reducing agent. Photocatalytic reduction of CO_2 by TEOA and **1**–**3** is hampered by the wrong site of electron localization in the one-electron reduced species $[\mathbf{1}]^-$–$[\mathbf{3}]^-$.

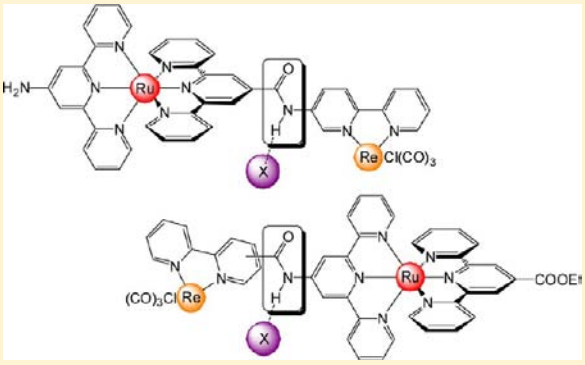

INTRODUCTION

By far the most studied and used photoactive coordination complex is $[Ru(bpy)_3]^{2+}$ and its derivatives due to its outstanding optical and (photo)chemical properties (bpy = 2,2′-bipyridine).[1,2] Important areas include applications as photosensitizers, as photocatalysts, and as molecular logic switches such as the encoder/decoder.[3−8] The field of bis(terpyridine) ruthenium(II) complexes $[Ru(tpy)_2]^{2+}$ (tpy = 2,2′;6′,2″-terpyridine) is considerably less exploited, although these complexes provide fewer stereochemical challenges[9] upon the introduction of substituents at the oligopyridine ligands (especially at the 4′ position) as compared to the chiral tris(bipyridine) counterparts. However, $[Ru(tpy)_2]^{2+}$ complexes feature low luminescence quantum yields and excited state lifetimes at room temperature in fluid solution. This often results in inefficient photoinduced electron transfer processes and hard to detect energy transfer processes under these conditions; e.g., energy transfer from iridium(III) to $[Ru(tpy)_2]^{2+}$ in multinuclear Ir^{III}∼Ru^{II} complexes at room temperature has been judged mainly from the absence of the iridium based emission.[10] The poor photochemistry of $[Ru(tpy)_2]^{2+}$ complexes is typically based on low energy ^{3}LF states of $[Ru(tpy)_2]^{2+}$, which lead to efficient deactivation of photoexcited luminescent ^{3}MLCT states. Two main strategies have emerged to energetically separate the ^{3}LF from the photoactive ^{3}MLCT states, namely lowering the ^{3}MLCT state by attaching electron withdrawing substituents at the terpyridine (X-tpy, X = SO_2Me, COOR)[11−16] and raising the ^{3}LF states by increasing the N–Ru–N bite angle to strengthen the ligand field.[17−24] We have introduced the push–pull substituted bis(terpyridine) ruthenium(II) amino acid complex **A** as a photoactive building block providing both room temperature emission in fluid solution (λ_{em} = 744 nm, Φ = 27.2 × 10^{-4}, τ = 34 ns) and functional groups (NH_2, COOH) at opposite directions for site selective modification and conjugation.[14]

The different addressable functional sites of **A** have been conjugated with organic α-amino acids,[16] with redox-active ferrocene derivatives as electron donors for photoinduced electron transfer processes,[14] with organic dyes as antenna units

Received: July 25, 2012
Published: January 11, 2013

dx.doi.org/10.1021/ic301632y | Inorg. Chem. 2013, 52, 1248−1264

Chart 1. Conjugates of Ruthenium Amino Acid A with Ferrocene,[14] Organic Dyes,[16] with Itself,[25] and with $ReCl(bpy)(CO)_3$ Fragments (This Work)

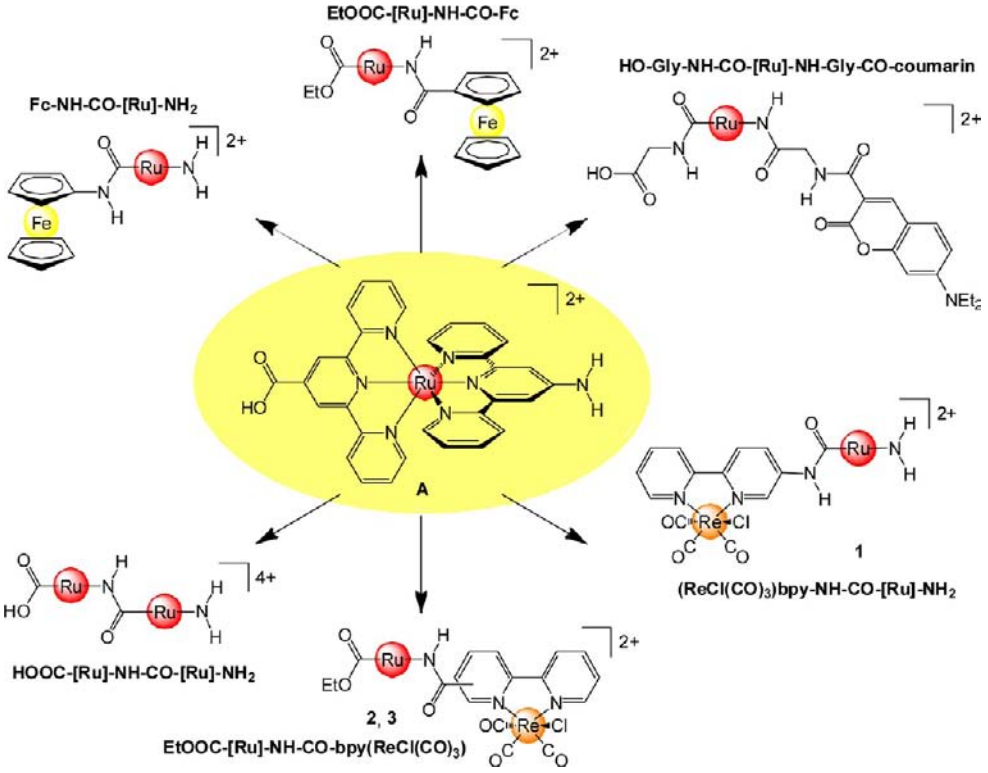

in the 400 nm region,[16] and with further ruthenium complexes with variable redox potentials giving mixed-valent systems for potential usage as molecular wires.[25] Furthermore, strategies have been developed to use solid-phase peptide synthesis techniques to construct larger arrays of redox and photoactive units, employing the achiral ruthenium amino acid **A** as a building block.[16] These procedures allow assembling inert metal complexes in a well-defined manner in peptidic architectures[14,16,26−28] similar to the famous ether-linked solution-built oligometallic complexes pioneered by Constable.[29]

In this study, we describe the conjugation of ruthenium amino acid **A** with 2,2′-bipyridine ligands at both the *N*- and the *C*-terminal end and using two different bpy attachment points (**L1**−**L3**). These amino acid bpy conjugates are then employed in a "complexes as ligands and complexes as metals" strategy[30] to give straightforward access to dinuclear systems with defined metal sequence. As first examples for the exploitation of metallo ligands **L1**−**L3** in this direction, we report the preparation of ruthenium∼rhenium binuclear amide-bridged complexes and their photophysical and redox properties (Chart 1). In contrast to chiral $[Ru(bpy)_3]^{2+}$ conjugates (Δ, Λ) the ruthenium part of **L1**−**L3** is achiral, and the formation of diastereomers in the directional binuclear complexes **1**−**3** is not an issue (*R*, *S* configuration of the Re fragment).[31]

The $ReCl(bpy)(CO)_3$ unit acts as a second photo- and redox-active unit in **1**−**3**.[32,33] Rhenium(I) diimine complexes have gained considerable interest in the field of electrocatalytic and photoinduced reduction of carbon dioxide.[34−50] The covalently linked combination of $[Ru(bpy)_3]^{2+}$ as a sensitizer and $ReCl(bpy)(CO)_3$ as a catalyst has been shown to be beneficial for the photocatalytic reduction of CO_2 with visible light.[51−58] In addition, luminescent rhenium(I) diimine complexes have found applications as sensors for metal cations, protons, or anions[59−63] as well as imaging agents and as cellular probes.[64,65]

A further interesting feature of amides **L1**−**L3** and **1**−**3** is the bridging CONH unit, which can engage in hydrogen bonding arrangements. Especially, the NH group of the positively charged complexes can act as a strong hydrogen atom donor in hydrogen bonds. Generally, amide hydrogen bonds play a decisive role in the stabilization of secondary structures in natural organic as well as in artificial inorganic/organometallic oligoamides[28,66,67] and in anion sensor devices based on metal complexes.[60,68−73] Furthermore, we have shown that anion coordination to specific sites in organometallic oligoamides can switch the preferred site of redox processes, e.g., from the *C*- to the *N*-terminus.[28,74] A prominent example of an amide connected sensitizer and proton reduction catalyst $[Ru(bpy)_2(phen\text{-}NHCO\text{-}bpy)PtCl_2]^{2+}$ has been devised by Sakai.[75] Interestingly, the "amide inverted" system $[Ru(bpy)_2(phen\text{-}CONH\text{-}bpy)PtCl_2]^{2+}$ is considerably less active.[76] A mononuclear water-oxidation catalyst appended with a $[Ru(bpy)_3]^{2+}$ sensitizer by an amide-linker has been reported by Meyer et al.[77]

With this in mind, we also have a closer look at amide orientation and anion coordination to the bridging amide with respect to the photo and redox properties of **L1**−**L3** and **1**−**3**. The interplay of the three functional units in **1**−**3**, namely the bis(terpyridine) ruthenium(II), the (bipyridine) rhenium(I), and the connecting amide bridge, will be addressed in the following.

dx.doi.org/10.1021/ic301632y | *Inorg. Chem.* 2013, 52, 1248−1264

EXPERIMENTAL SECTION

General Considerations. Chemicals were obtained from commercial suppliers and used without further purification. CO_2 was obtained from Westfalen AG, Germany (Protadur E290). Bis-(terpyridine) ruthenium(II) complexes **A** and **B**[14] were synthesized as reported. IR spectra were recorded on a BioRad Excalibur FTS 3000 spectrometer using cesium iodide disks and KBr cells in CH_3CN. UV/vis spectra were recorded on a Varian Cary 5000 spectrometer in 1.0 cm cells (Hellma, suprasil). Emission spectra were recorded on a Varian Cary Eclipse spectrometer. Quantum yields were determined by comparing the areas under the emission spectra on an energy scale [cm^{-1}] recorded for optically matched solutions of the samples and the reference ($[Ru(bpy)_3]^{2+}$, Φ = 0.062 (older value)[78]/0.095 (corrected value)[79]) in CH_3CN. As $\Phi(\mathbf{B}) = 18 \times 10^{-4}$ (**B** is the ethyl ester of **A**)[14] was given with respect to the older reference value $\Phi([Ru(bpy)_3]^{2+}) = 0.062$ (older value), the quantum yield of **B** has to be adjusted to $\Phi(\mathbf{B}) = 27.6 \times 10^{-4}$ for comparison. Experimental uncertainty is 15%. ESI mass spectra were recorded with a Finnigan TSQ 700 triple-quadrupole or a Q-Tof Ultima API mass spectrometer (Micromass/Waters) with analyte solutions in acetonitrile. NMR spectra were obtained on a Bruker Avance II 400 spectrometer at 400.31 MHz (^1H) and 100.66 MHz ($^{13}C\{^1H\}$) at 25 °C. Chemical shifts (δ/ppm) are reported with respect to residual solvent peaks as internal standards: CD_3CN $\delta(^1H)$ = 1.94 ppm, $\delta(^{13}C)$ = 1.24 ppm. s = singlet, d = doublet, dd = doublet of doublets, m = multiplet, and pt = pseudo-triplet (unresolved doublet of doublets). Electrochemical experiments were carried out on a BioLogic SP-50 voltammetric analyzer using platinum wire working and counter electrodes and a 0.01 M $Ag/AgNO_3$ electrode as a reference electrode. The measurements were carried out at a scan rate of 100 mV s^{-1} for cyclic voltammetry experiments and at 10 mV s^{-1} for square wave voltammetry experiments using 0.1 M $[n\mathrm{Bu_4N}][PF_6]$ as a supporting electrolyte in CH_3CN. Potentials are given relative to the ferrocene/ferrocenium couple ($E_{1/2}$ = 90 ± 5 mV under the experimental conditions). X-band CW EPR spectra were measured on a Miniscope MS 300 (Magnettech GmbH, Germany). g values are referenced to external Mn^{2+} in ZnS (g = 2.118, 2.066, 2.027, 1.986, 1.946, 1.906). Simulations were performed with the program package EasySpin.[80] Elemental analyses were performed by the microanalytical laboratory of the chemical institutes of the University of Mainz.

Crystal Structure Determinations. Intensity data were collected with a Bruker AXS Smart1000 CCD diffractometer with an APEX II detector and an Oxford cooling system and corrected for absorption and other effects using Mo Kα radiation (λ = 0.71073 Å). The diffraction frames were integrated using the SAINT package, and most were corrected for absorption with MULABS.[81,82] The structures were solved by direct methods and refined by the full-matrix least-squares method based on F^2 using the SHELXTL software package.[83,84] All non-hydrogen atoms were refined anisotropically while the positions of most hydrogen atoms were generated with appropriate geometric constraints and allowed to ride on their respective parent carbon atoms with fixed isotropic thermal parameters. CCDC-885078 (**L2**·2.4CH_3CN) and CCDC-885077 (**L3**·HPF_6·2H_2O) contain the supplementary crystallographic data for this paper. These data can be obtained free of charge from The Cambridge Crystallographic Data Centre via www.ccdc.cam.ac.uk/data_request/cif.

Crystallographic Data of ***L2***·2.4CH_3CN. $C_{48.80}H_{40.20}F_{12}N_{11.40}O_3P_2Ru$ (1225.33); T = 293(2) K; triclinic; $P\bar{1}$; a = 13.7348(11) Å, b = 14.1615(11) Å, c = 16.3271(16) Å, α = 91.869(3)°, β = 108.135(2)°, γ = 117.222(2)°; V = 2625.5(4) Å^3; Z = 2; density, calcd. = 1.550 g/cm^3, μ = 0.456 mm^{-1}; F(000) = 1238; crystal size, 0.44 × 0.29 × 0.19 mm; θ = 2.33 to 28.06°; $-18 \le h \le 18$, $-18 \le k \le 18$, $-21 \le l \le 21$; rfln collected = 57757; rfln unique = 12695 [R(int) = 0.0639]; completeness to θ = 28.06 = 99.5%; semiempirical absorption correction from equivalents; max. and min transmission, 0.976 and 0.853; data, 12 695; restraints, 0; parameters, 780; goodness-of-fit on F^2 = 0.976; final R indices [$I > 2\sigma(I)$] R_1 = 0.0467, wR_2 = 0.1252; R indices (all data) R_1 = 0.0665, wR_2 = 0.1355; largest diff. peak and hole, 0.902 and −0.834 e Å^{-3}.

Crystallographic Data of ***L3***·HPF_6·2H_2O. $C_{44}H_{38}F_{18}N_9O_3P_3Ru$ (1308.81); T = 173(2) K; triclinic; $P\bar{1}$; a = 8.8053(5) Å, b = 10.0981(6) Å, c = 28.5084(17) Å, α = 79.995(2)°, β = 87.198(2)°, γ = 88.736(2)°; V = 2493.1(3) Å^3; Z = 2; density, calcd. = 1.743 g/cm^3, μ = 0.535 mm^{-1}; F(000) = 1312; crystal size, 0.22 × 0.15 × 0.02 mm; θ = 2.30 to 28.01°; $-11 \le h \le 11$, $-13 \le k \le 13$, $-37 \le l \le 37$; rfln collected = 61 310; rfln unique = 11967 [R(int) = 0.1204]; completeness to θ = 28.01 = 99.2%; semiempirical absorption correction from equivalents; max. and min transmission, 0.9894 and 0.8914; data, 11 967; restraints, 68; parameters, 799; goodness-of-fit on F^2 = 0.864; final R indices [$I > 2\sigma(I)$] R_1 = 0.0475, wR_2 = 0.0746; R indices (all data) R_1 = 0.1058, wR_2 = 0.0866; largest diff. peak and hole, 0.525 and −0.762 e Å^{-3}.

Computational Details. Density functional calculations were carried out with the Gaussian 09/DFT[85] series of programs. The B3LYP formulation of density functional theory was used employing the LANL2DZ basis set as implemented in Gaussian 09.[85] To include solvent effects, the integral equation formalism polarizable continuum model (IEFPCM, CH_3CN) was employed as implemented in Gaussian 09.[85] All structures were characterized as minima by frequency analysis (N_{imag} = 0). No symmetry constraints were imposed on the molecules.

Photocatalytic Reduction Experiments. Catalysis test experiments were performed in a Schlenk tube containing a CH_3CN/TEOA (5:1) solution of the metal complexes (1 mM) after purging with CO_2 for 20 min. Experiments were also done in the presence of the sacrificial electron donor (1-benzyl-1,4-dihydronicotinamide, BNAH, 0.1 M). The solutions were irradiated at 400 or 470 nm using LED torches. All experiments were conducted at ambient temperature. Gas samples were analyzed using a Hewlett-Packard gas chromatograph HP 5890 A equipped with a thermal conductivity detector and an Agilent Technologies column HP-PLOT MS 5 Å 30m × 0.53 mm ID × 25 μm film, DB-624. The oven was operated for 2 min at 50 °C after injection and then heated to 200 °C with 10 K min^{-1}. After irradiation for 6 h, gas samples (250 μL) were withdrawn and injected into the gas chromatograph using a gastight syringe.

Synthesis of ***L1***. Ruthenium amino acid **A**[14] (150 mg, 0.16 mmol) was dissolved in dry acetonitrile (20 mL). HATU (2-(7-aza-1H-benzotriazole-1-yl)-1,1,3,3-tetramethyluronium hexafluorophosphate; 112 mg, 0.30 mmol), dry triethylamine (0.06 mL), and 5-amino-2,2′-bipyridine[86−88] (51 mg, 0.30 mmol) were added, and the solution was stirred at 22 °C for 18 h and at 50 °C for 2 h. After cooling to room temperature, the solvent was removed under reduced pressure, and the crude product was dissolved in acetonitrile (3 mL), and $[NH_4][PF_6]$ (500 mg, 3.07 mmol) in water (3 mL) was added. After the addition of water (100 mL), the precipitate was collected by filtration, washed with water (20 mL) and diethyl ether (100 mL), and dried in a vacuum. **L1** was obtained as a red powder (144 mg, 0.13 mmol, 82%). ^1H NMR (CD_3CN): δ = 9.63 (s, 1H, NH), 9.19−9.18 (m, 3H, H^9/H^{2}), 8.70 (d, $^3J_{HH}$ = 4.4 Hz, 1H, H^{18}), 8.63 (d, $^3J_{HH}$ = 8.2 Hz, 2H, H^5), 8.58 (d, $^3J_{HH}$ = 8.9 Hz, 1H, H^{12}), 8.52 (dd, $^3J_{HH}$ = 8.5 Hz, $^4J_{HH}$ = 2.4 Hz, 1H, H^{11}), 8.45 (d, $^3J_{HH}$ = 7.8 Hz, 1H, H^{15}), 8.28 (d, $^3J_{HH}$ = 8.2 Hz, 2H, $H^{5'}$), 8.00−7.91 (m, 5H, $H^6/H^{2'}/H^{16}$), 7.86 (pt, 2H, $H^{6'}$), 7.59 (d, $^3J_{HH}$ = 5.5 Hz, 2H, H^8), 7.42 (pt, 1H, H^{17}), 7.29 (pt, 2H, H^7), 7.22 (d, $^3J_{HH}$ = 5.5 Hz, 2H, $H^{8'}$), 7.06 (pt, 2H, $H^{7'}$), 6.00 (s, 2H, NH_2). $^{13}C\{^1H\}$ NMR (CD_3CN): δ = 164.1 (s, CONH), 159.2 (s, $C^{4'}$), 158.9 (s, C^4), 157.7 (s, C^3), 156.9 (s, $C^{1'}$), 156.3 (s, C^{14}), 154.9 (s, $C^{3'}$), 153.6 (s, $C^{8'}$), 153.1 (s, C^8/C^{13}), 150.2 (s, C^{18}), 142.2 (s, C^9), 139.7 (s, C^1), 139.0 (s, $C^{6'}$), 138.8 (s, C^6), 138.1 (s, C^{16}), 136.3 (s, C^{10}), 129.3 (s, C^{11}), 128.7 (s, C^7), 128.0 (s, C^{17}), 127.9 (s, $C^{7'}$), 125.3 (s, C^5), 124.7 (s, $C^{5'}$), 122.3 (s, C^2), 121.8 (s, C^{12}), 121.3 (s, C^{15}), 109.5 (s, $C^{2'}$). ESI-MS: m/z (%) = 925.1 (100) $[M+PF_6]^+$, 390.1 (30) $[M]^{2+}$. IR (CsI): $\tilde{\nu}$ 3400 (m, NH), 3234 (w, NH), 3084 (w, CH), 1686 (m, amide I), 1525 (m, amide II), 1246 (m), 837 cm^{-1} (vs, PF). Elemental analysis calcd (%) for $C_{41}H_{30}F_{12}N_{10}OP_2Ru$ (1069.74): C, 46.03; H, 2.83; N, 13.09. Found: C, 45.77; H, 2.55; N, 12.87.

Synthesis of ***L2***. 2,2′-Bipyridine-5-carboxylic acid chloride[89] (116 mg, 0.53 mmol) was dissolved in dry dichloromethane (10 mL). Ruthenium amino acid ester **B**[14] (250 mg, 0.27 mmol) dissolved in dry acetonitrile (15 mL) was added, and the mixture was stirred for 12 h at

dx.doi.org/10.1021/ic301632y | Inorg. Chem. 2013, 52, 1248−1264

40 °C. After cooling to room temperature, the solvent was removed under reduced pressure. The crude product was dissolved in acetonitrile (3 mL), and $[NH_4][PF_6]$ (500 mg, 3.07 mmol) in water (3 mL) was added. After the addition of water (100 mL), the precipitate was collected by filtration, washed with water (20 mL) and diethyl ether (100 mL), and dried in a vacuum. **L2** was obtained as a red powder (280 mg, 0.25 mmol, 93%). Crystals suitable for X-ray diffraction were obtained by dissolving **L2** in acetonitrile/dichloromethane and slow evaporation of the solvent in a toluene atmosphere. ^{1}H NMR (CD_3CN): δ = 10.05 (s, 1H, NH), 9.39 (s, 1H, H^9), 9.20 (s, 4H, $H^2/H^{2\prime}$), 8.77 (d, $^3J_{HH}$ = 4.0 Hz, 1H, H^{18}), 8.72−8.65 (m, 3H, H^{12}/H^5), 8.61−8.56 (m, 2H, H^{11}/H^{15}), 8.45 (d, $^3J_{HH}$ = 8.1 Hz, 2H, $H^{5\prime}$), 8.02−7.91 (m, 5H, $H^{16}/H^6/H^{6\prime}$), 7.52−7.49 (m, 3H, H^{17}/H^8), 7.30 (d, $^3J_{HH}$ = 5.1 Hz, 2H, $H^{8\prime}$), 7.25 (pt, 2H, H^7), 7.14 (pt, 2H, $H^{7\prime}$), 4.66 (q, $^3J_{HH}$ = 7.0 Hz, 2H, CH_2), 1.58 (t, $^3J_{HH}$ = 7.0 Hz, 3H, CH_3). $^{13}C\{^1H\}$ NMR (CD_3CN): δ = 166.5 (s, CONH), 165.0 (s, COO), 160.1 (s, C^{13}), 158.6 (s, $C^{4\prime}$), 158.6 (s, C^4), 157.4 (s, C^3), 156.0 (s, $C^{3\prime}$), 155.6 (s, C^{14}), 153.8 (s, $C^{8\prime}$), 153.3 (s, C^8), 150.5 (s, C^{18}), 149.9 (s, C^9), 147.8 (s, $C^{1\prime}$), 139.4 (s, $C^{6\prime}$), 139.1 (s, C^6), 138.5 (s, C^{16}), 137.7 (s, C^{11}), 137.2 (s, C^1), 130.2 (s, C^{10}), 128.8 (s, C^7), 128.5 (s, $C^{7\prime}$), 125.9 (s, C^{17}), 125.8 (s, C^5), 125.4 (s, $C^{5\prime}$), 123.6 (s, C^2), 122.5 (s, C^{15}), 121.5 (s, C^{12}), 114.9 (s, $C^{2\prime}$), 63.8 (s, CH_2), 14.6 (s, CH_3). ESI-MS: m/z (%) = 982.1 (100) $[M+PF_6]^+$, 418.6 (34) $[M]^{2+}$. IR (CsI): $\tilde{\nu}$ 3406 (w, NH), 3110 (w, CH), 1725 (s, CO_{ester}), 1689 (m, amide I), 1525 (m, amide II), 1258 (s), 843 cm^{-1} (vs, PF). Elemental analysis calcd (%) for $C_{44}H_{33}F_{12}N_9O_3P_2Ru\cdot H_2O$ (1144.80): C, 46.16; H, 3.08; N, 11.01. Found: C, 46.04; H, 2.89; N, 10.76.

Synthesis of ***L3***. 2,2′-Bipyridine-4-carboxylic acid chloride[89] (116 mg, 0.53 mmol) was dissolved in dry dichloromethane (10 mL). Ruthenium amino acid ester **B**[14] (250 mg, 0.27 mmol) dissolved in dry acetonitrile (15 mL) was added, and the solution was stirred for 12 h at 40 °C. After cooling to room temperature, the solvent was removed under reduced pressure. The crude product was dissolved in acetonitrile (3 mL), and $[NH_4][PF_6]$ (500 mg, 3.07 mmol) in water (3 mL) was added. After the addition of water (100 mL), the precipitate was collected by filtration, washed with water (20 mL) and diethyl ether (100 mL), and dried in a vacuum. **L3** was obtained as a red powder (270 mg, 0.24 mmol, 90%). Crystals suitable for X-ray diffraction were obtained by dissolving **L3** in acetonitrile/dichloromethane and slow evaporation of the solvent in a toluene atmosphere. ^{1}H NMR (CD_3CN): δ = 10.11 (s, 1H, NH), 9.20−9.18 (m, 4H, $H^2/H^{2\prime}$), 9.13 (d, $^3J_{HH}$ = 4.8 Hz, 1H, H^9), 8.97 (s, 1H, H^{12}), 8.87 (d, $^3J_{HH}$ = 5.1 Hz, 1H, H^{18}), 8.76 (d, $^3J_{HH}$ = 8.1 Hz, 1H, H^{15}), 8.67 (d, $^3J_{HH}$ = 8.1 Hz, 2H, H^5), 8.55 (pt, 1H, H^{16}), 8.45 (d, $^3J_{HH}$ = 8.1 Hz, 2H, $H^{5\prime}$), 8.24 (d, $^3J_{HH}$ = 4.0 Hz, 1H, H^{10}), 7.99−7.92 (m, 5H, $H^6/H^{6\prime}/H^{17}$), 7.48 (d, $^3J_{HH}$ = 5.1 Hz, 2H, H^8), 7.31 (d, $^3J_{HH}$ = 5.1 Hz, 2H, $H^{8\prime}$), 7.25 (pt, 2H, H^7), 7.15 (pt, 2H, $H^{7\prime}$), 4.66 (q, $^3J_{HH}$ = 7.0 Hz, 2H, CH_2), 1.58 (t, $^3J_{HH}$ = 7.0 Hz, 3H, CH_3). $^{13}C\{^1H\}$ NMR (CD_3CN): δ = 165.6 (s, CONH), 164.9 (s, COO), 158.5 (s, $C^{4\prime}$), 158.5 (s, C^4), 157.3 (s, C^3), 156.1 (s, $C^{3\prime}$), 153.8 (s, $C^{8\prime}$), 153.3 (s, C^8), 151.9 (s, C^9), 150.4 (s, C^{13}), 150.3 (s, C^{14}) 147.2 (s, $C^{1\prime}$), 145.7 (s, C^{16}), 145.6 (s, C^{18}) 144.1 (s, C^{11}), 139.3 (s, $C^{6\prime}$), 139.0 (s, C^6), 137.3 (s, C^1), 128.7 (s, C^7), 128.5 (s, $C^{7\prime}$), 127.9 (s, C^{17}), 125.8 (s, C^5), 125.4 (s, $C^{5\prime}$), 125.1 (s, C^{10}), 124.3 (s, C^{15}), 123.6 (s, C^2), 120.9 (s, C^{12}), 115.0 (s, $C^{2\prime}$), 63.8 (s, CH_2), 14.5 (s, CH_3). ESI-MS: m/z (%) = 982.3 (100) $[M+PF_6]^+$, 418.8 (35) $[M]^{2+}$. IR (CsI): $\tilde{\nu}$ 3117 (w, CH), 1737 (m, CO_{ester}), 1685 (m, amide I), 1531 (m, amide II), 1249 (s), 844 cm^{-1} (vs, PF). Elemental analysis calcd (%) for $C_{44}H_{33}F_{12}N_9O_3P_2Ru\cdot 8H_2O$ (1468.51): C, 41.58; H, 3.89; N, 9.92. Found: C, 41.68; H, 3.80; N, 9.95.

Synthesis of ***1***. Metallo ligand **L1** (128 mg, 0.12 mmol) and $ReCl(CO)_5$ (56 mg, 0.16 mmol) were dissolved in dry acetonitrile (15 mL) and heated under reflux for 18 h. After cooling to room temperature, the solvent was removed under reduced pressure, and the crude product was suspended in ethanol (20 mL) by ultrasonic treatment. After filtration, the red residue was washed with ethanol (20 mL) and diethyl ether (100 mL) and dried in a vacuum. Mixed-metal complex **1** was obtained as a red powder in 84% yield (139 mg, 0.10 mmol). ^{1}H NMR (CD_3CN): δ = 10.14 (s, 1H, NH), 9.76 (d, $^4J_{HH}$ = 2.0 Hz, 1H, H^9),9.26 (s, 2H, H^2), 9.04 (d, $^3J_{HH}$ = 5.1 Hz, 1H, H^{18}), 8.84 (dd, $^3J_{HH}$ = 8.9 Hz, $^4J_{HH}$ = 2.0 Hz, 1H, H^{11}), 8.67 (d, $^3J_{HH}$ = 7.8 Hz, 2H, H^5), 8.51 (d, $^3J_{HH}$ = 8.9 Hz, 1H, H^{12}), 8.43 (d, $^3J_{HH}$ = 8.2 Hz, 1H, H^{15}), 8.29−8.21 (m, 3H, $H^{5\prime}/H^{16}$), 8.00−7.95 (m, 4H, $H^6/H^{2\prime}$), 7.86 (pt, 2H, $H^{6\prime}$) 7.66−7.58 (m, 3H, H^{17}/H^8), 7.29 (pt, 2H, H^7), 7.22 (d, $^3J_{HH}$ = 5.5 Hz, 2H, $H^{8\prime}$), 7.07 (pt, 2H, $H^{7\prime}$), 6.02 (s, 2H, NH_2). $^{13}C\{^1H\}$ NMR (CD_3CN): δ = 164.5 (s, CONH), 159.2 (s, $C^{4\prime}$), 158.9 (s, C^4), 157.9 (s, C^3), 156.9 (s, $C^{1\prime}$), 156.2 (s, C^{14}), 154.8 (s, $C^{3\prime}$), 153.9 (s, C^{18}), 153.7 (s, $C^{8\prime}$), 153.1 (s, C^8), 152.0 (s, C^{13}), 145.2 (s, C^9), 140.9 (s, C^{16}), 139.4 (s, C^{10}), 139.0 (s, $C^{6\prime}$), 138.8 (s, C^6), 138.8 (s, C^1), 130.6 (s, C^{11}), 128.8 (s, C^7), 128.0 (s, C^{17}), 127.9 (s, $C^{7\prime}$), 125.4 (s, C^{12}/C^5), 124.7 (s, $C^{5\prime}$), 124.6 (s, C^{15}), 122.4 (s, C^2), 109.5 (s, $C^{2\prime}$). ESI-MS: m/z (%) = 1231.1 (34) $[M+PF_6]^+$, 543.1 (100) $[M]^{2+}$. IR (CsI): $\tilde{\nu}$ 3404 (w, NH), 3086 (w, CH), 2023 (vs, CO_{Re}), 1917 (vs, CO_{Re}), 1898 (vs, CO_{Re}), 1686 (w, amide I), 1535 (m, amide II), 1236 (m, CO), 840 (vs, PF). IR (CH_3CN): $\tilde{\nu}$ 3370 (w, NH), 2022 (s, CO_{Re}), 1915 (s, CO_{Re}), 1900 (s, CO_{Re}), 1680 (w, amide I), 1238 (w, CO), 849 cm^{-1} (vs, PF). Elemental analysis calcd (%) for $C_{44}H_{30}ClF_{12}N_{10}O_4P_2ReRu$ (1375.43): C, 38.42; H, 2.20; N, 10.18. Found: C, 38.92; H, 2.14; N, 10.16.

Synthesis of ***2***. Metallo ligand **L2** (150 mg, 0.13 mmol) and $ReCl(CO)_5$ (58 mg, 0.16 mmol) were dissolved in dry acetonitrile (15 mL) and heated under reflux for 2 days. After cooling to room temperature, the solvent was removed under reduced pressure, and the crude product was suspended in ethanol (20 mL) by ultrasonic treatment. After filtration, the red residue was washed with ethanol (20 mL) and diethyl ether (100 mL) and dried in a vacuum. Mixed metal complex **2** was obtained as a red powder in 73% yield (140 mg, 0.10 mmol). ^{1}H NMR (CD_3CN): δ = 10.28 (s, 1H, NH), 9.60 (d, $^4J_{HH}$ = 1.7 Hz, 1H, H^9), 9.20 (s, 2H, H^2), 9.15−9.12 (m, 3H, $H^{2\prime}/H^{18}$), 8.82 (dd, $^3J_{HH}$ = 8.5 Hz, $^4J_{HH}$ = 2.0 Hz, 1H, H^{11}), 8.69−8.66 (m, 3H, H^{12}/H^5), 8.60 (d, $^3J_{HH}$ = 8.2 Hz, 1H, H^{15}), 8.47 (d, $^3J_{HH}$ = 8.2 Hz, 2H, $H^{5\prime}$), 8.31 (pt, 1H, H^{16}), 7.99−7.91 (m, 4H, $H^6/H^{6\prime}$), 7.75 (pt, 1H, H^{17}), 7.49 (d, $^3J_{HH}$ = 5.5 Hz, 2H, H^8), 7.30 (d, $^3J_{HH}$ = 5.1 Hz, 2H, $H^{8\prime}$), 7.22 (pt, 2H, H^7), 7.14 (pt, 2H, $H^{7\prime}$), 4.66 (q, $^3J_{HH}$ = 7.2 Hz, 2H, CH_2), 1.58 (t, $^3J_{HH}$ = 7.2 Hz, 3H, CH_3). $^{13}C\{^1H\}$ NMR (CD_3CN): δ = 164.9 (s, COO), 164.2 (s, CONH), 159.5 (s, C^{13}), 158.5 (s, $C^4/C^{4\prime}$), 157.3 (s, C^3), 156.1 (s, $C^{3\prime}$), 155.5 (s, C^{14}), 154.3 (s, C^{18}), 153.7 (s, $C^{8\prime}$), 153.4 (s, C^8), 153.1 (s, C^9), 147.3 (s, $C^{1\prime}$), 141.1 (s, C^{16}), 140.5 (s, C^{11}), 139.3 (s, $C^{6\prime}$), 139.0 (s, C^6), 137.3 (s, C^1), 133.6 (s, C^{10}), 129.3 (s, C^{17}), 128.7 (s, C^7), 128.5 (s, $C^{7\prime}$), 126.1 (s, C^{15}), 125.8 (s, C^5), 125.5 (s, $C^{5\prime}$), 125.0 (s, C^{12}), 123.6 (s, C^2), 114.9 (s, $C^{2\prime}$), 63.8 (s, CH_2), 14.5 (s, CH_3). ESI-MS: m/z (%) = 1288.2 (100) $[M+PF_6]^+$, 1142.2 (10) $[M]^+$, 553.6 (67) $[M-Cl]^{2+}$. IR (CsI): $\tilde{\nu}$ 3110 (w, CH), 2025 (vs, CO_{Re}), 1921 (vs, CO_{Re}), 1899 (vs, CO_{Re}), 1725 (s, CO_{ester}), 1693 (m, amide I), 1527 (m, amide II), 1257 (s, CO), 841 (vs, PF). IR (CH_3CN): $\tilde{\nu}$ 3380 (w, NH), 2023 (s, CO_{Re}), 1919 (s, CO_{Re}), 1902 (s, CO_{Re}), 1726 (w, CO_{ester}), 1692 (w, amide II), 1254 (m, CO_{val}), 849 cm^{-1} (vs, PF). Elemental analysis calcd (%) for $C_{47}H_{33}ClF_{12}N_9O_6P_2ReRu\cdot 2H_2O$ (1468.51): C, 38.44; H, 2.54; N, 8.58. Found: C, 38.42; H, 2.31; N, 8.80.

Synthesis of ***3***. Metallo ligand **L3** (150 mg, 0.13 mmol) and $ReCl(CO)_5$ (58 mg, 0.16 mmol) were dissolved in dry acetonitrile (15 mL) and heated under reflux for 2 days. After cooling to room temperature, the solvent was removed under reduced pressure, and the crude product was suspended in ethanol (20 mL) by ultrasonic treatment. After filtration, the red residue was washed with ethanol (20 mL) and diethyl ether (100 mL) and dried in a vacuum. Mixed-metal complex **3** was obtained as a red powder in 69% yield (129 mg, 0.09 mol). ^{1}H NMR (CD_3CN): δ = 12.39 (s, 1H, NH), 9.91 (s, 2H, $H^{2\prime}$), 9.61 (s, 1H, H^{12}), 9.20−9.11 (m, 4H, $H^2/H^{15}/H^9$), 8.88 (d, $^3J_{HH}$ = 5.5 Hz, 1H, H^{18}), 8.80 (d, $^3J_{HH}$ = 7.8 Hz, 2H, $H^{5\prime}$), 8.67−8.62 (m, 3H, H^5/H^{10}), 8.11 (pt, 1H, H^{16}), 7.96 (pt, 2H, H^6), 7.80 (pt, 2H, $H^{6\prime}$), 7.56 (d, $^3J_{HH}$ = 5.5 Hz, 2H, H^8), 7.32−7.24 (m, 5H, $H^{17}/H^7/H^{8\prime}$), 7.05 (pt, 2H, $H^{7\prime}$), 7.65 (q, $^3J_{HH}$ = 7.2 Hz, 2H, CH_2), 1.58 (t, $^3J_{HH}$ = 7.2 Hz, 3H, CH_3). $^{13}C\{^1H\}$ NMR (CD_3CN): δ = 165.0 (s, COO), 164.4 (s, CONH), 159.1 (s, $C^{4\prime}$), 158.5 (s, C^4), 157.9 (s, C^{13}), 157.3 (s, C^3), 156.1 (s, C^{14}), 155.9 (s, $C^{3\prime}$), 154.6 (s, C^9), 153.6 (s, C^{18}), 153.4 (s, $C^8/C^{8\prime}$), 148.4 (s, $C^{1\prime}$), 144.1 (s, C^{11}), 140.9 (s, C^{16}), 139.2 (s, $C^{6\prime}$), 138.9 (s, C^6), 137.0 (s, C^1), 128.8 (s, C^7), 128.4 (s, C^{17}), 128.2 (s, $C^{7\prime}$), 127.4 (s, C^{10}), 126.8 (s, C^{15}), 125.8 (s, $C^{5\prime}$), 125.7 (s, C^5), 123.5

dx.doi.org/10.1021/ic301632y | *Inorg. Chem.* 2013, 52, 1248−1264

Scheme 1. Synthesis of Metallo Ligands L1−L3 and Atom Numbering Used for NMR Assignments

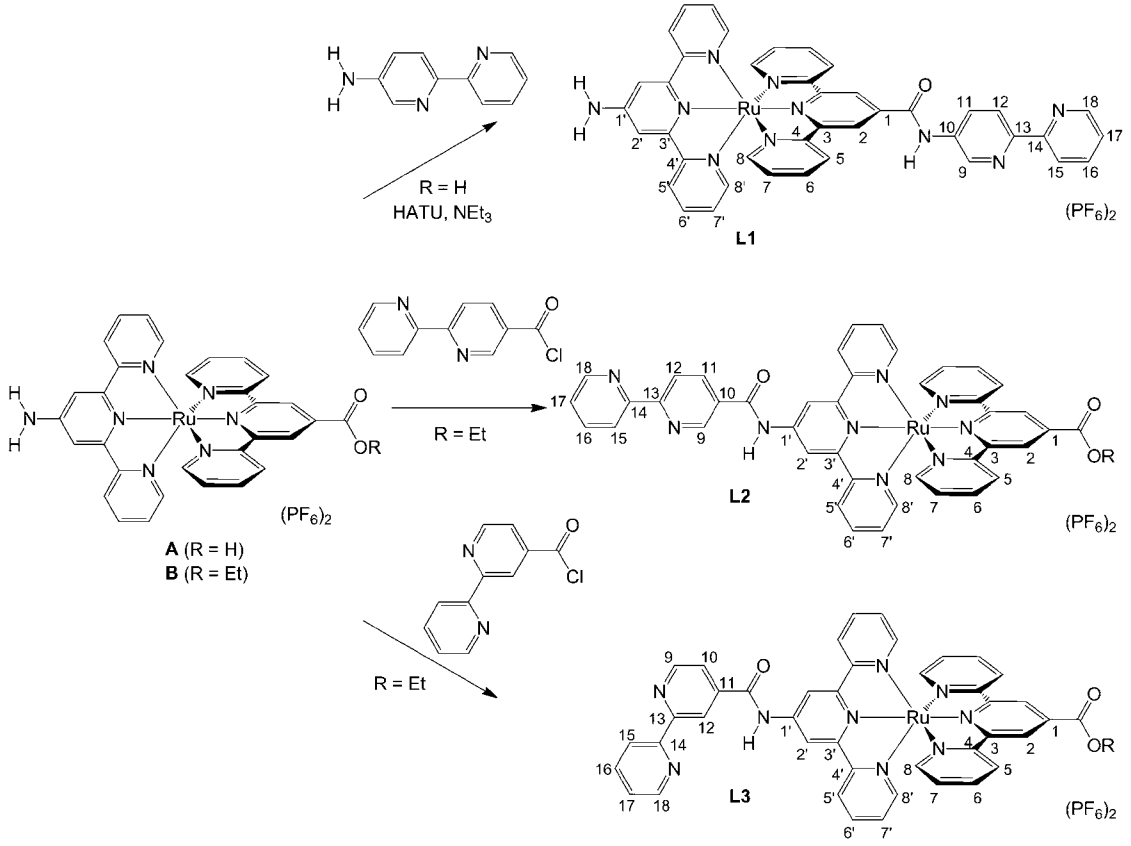

Table 1. Photophysical Properties of L1−L3 and 1−3 in Deaerated CH_3CN at Room Temperature and Emission at 77 K in Butyronitrile

	absorption λ_{max}/nm (ε/M^{-1} cm^{-1})			emission		
	$^1(\pi-\pi^*$, ligands)	^{1}MLCT(Ru)	^{1}MLCT(Re)[a]	λ_{em}/nm (λ_{exc}/nm) at 300 K	$\Phi/\times10^{4}$[b]	λ_{em}/nm (λ_{exc}/nm) at 77 K
L1	279 (58190), 305 (58160)	500 (23480)		727 (500)	15.0	651 (490)
L2	276 (59170), 307 (72930)	492 (25970)		674 (492)	15.8	653 (490)
L3	276 (77820), 309 (56750)	493 (24440)		673 (493)	16.6	653 (490)
1	275 (56650), 307 (50180)	502 (21840)	353 (sh)	739 (502)	11.0	657 (490)
2	276 (64260), 308 (72960)	494 (27660)	367 (sh)	674 (494)	18.5	653 (494)
3	275 (61570), 309 (58530)	496 (27810)	362 (sh)	678 (496)	14.4	653 (500)

[a]From the difference spectra of **1**−**L1**, **2**−**L2**, and **3**−**L3**, respectively. [b]With respect to the reference value $\Phi([Ru(bpy)_3]^{2+})$ = 0.095 in deaerated CH_3CN at room temperature.[79]

(s, C^2), 123.3 (s, C^{12}), 115.9 (s, $C^{2'}$), 63.7 (s, CH_2), 14.5 (s, CH_3). ESI-MS: m/z (%) = 1288.0 (100) $[M+PF_6]^+$, 553.5 (43) $[M-Cl]^{2+}$. IR (CsI): $\tilde{\nu}$ 3096 (w, CH), 2027 (s, CO_{Re}), 1926 (s, CO_{Re}), 1894 (s, CO_{Re}), 1728 (s, CO_{ester}), 1701 (m, amide I), 1526 (s, amide II), 1258 (s, CO), 839 (vs, PF). IR (CH_3CN): $\tilde{\nu}$ 3376 (w, NH), 2023 (vs, CO_{Re}), 1919 (s, CO_{Re}), 1902 (s, CO_{Re}), 1726 (w, CO_{ester}), 1682 (w, amide I), 1254 (m, CO), 849 cm^{-1} (vs, PF). Elemental analysis calcd (%) for $C_{47}H_{33}ClF_{12}N_9O_6P_2ReRu$ (1432.48): C, 39.38; H, 2.39; N, 8.79. Found: C, 39.57; H, 2.33; N, 8.97.

RESULTS AND DISCUSSION

Amide Coupling and Properties of Metallo Ligands L1−L3. The metallo ligand **L1** is assembled from ruthenium amino acid **A**[14] and 5-amino-2,2′-bipyridine[86−88] by activation with HATU [2-(7-aza-1H-benzotriazole-1-yl)-1,1,3,3-tetramethyluronium hexafluorophosphate] (Scheme 1). Due to the extremely low reactivity of the NH_2 group of the dicationic ruthenium(II) complex **A**, there is no need for protecting group chemistry.[14] Thus, selective amide bond formation between the amino bipyridine and the amino acid is easily achieved. The linear and bent metallo ligands **L2** and **L3** were built from ruthenium amino acid ester **B**[14] and 4- or 5-substituted bipyridine 5-carboxylic acid,[89] respectively. The bpy acids were activated as acid chlorides by thionyl chloride to achieve reasonable coupling yields with the poorly reactive amino group of **B**. Using these coupling protocols, all metallo ligands **L1**−**L3** were obtained as red powders in coupling yields above 80%.

ESI mass spectra indicate the correct formation of the amide bonds as ion peaks corresponding to the coupling products $[M+PF_6]^+$ and $[M]^{2+}$ with expected isotopic distribution patterns are observed in each case. Most ^{1}H NMR resonances of amino acid **A**[14] are essentially unaffected by the bpy attachment to give **L1**. However, resonances H^9 and H^{11} of 5-amino-bipyridine are shifted in the metallo ligand **L1** from δ = 8.12

dx.doi.org/10.1021/ic301632y | Inorg. Chem. 2013, 52, 1248−1264

and δ = 7.09 (5-NH_2-bpy[86]) to δ = 9.18 and δ = 8.52 ppm (**L1**), respectively. The amide NH resonance of **L1** is found at δ = 9.63 ppm. The ^{13}C resonances C^1 and C^2 of the tpy ligand are shifted from δ = 135.6 ppm (**A**[14]) to δ = 139.7 ppm and from δ = 125.0 ppm (**A**[14]) to δ = 122.3 ppm, respectively.

Similarly, most ^{1}H NMR resonances of amino acid ester **B** are unaffected by bpy conjugation to give **L2** and **L3**. Importantly, the resonance of the two NH_2 protons at δ = 6.00 ppm (**B**[14]) is replaced by amide NH resonances at δ = 10.05 (**L2**) and δ = 10.11 ppm (**L3**). The singlet of the tpy protons $H^{2'}$ adjacent to the amide group are significantly shifted to higher frequency from δ = 7.96 ppm (**B**[14]) to δ = 9.20 ppm (**L2**, **L3**). The ^{13}C resonances $C^{1'}$ and $C^{2'}$ of the *N*-substituted tpy ligand are shifted from δ = 154.4 ppm (**B**[14]) to δ = 147.8 (**L2**) and δ = 147.2 ppm (**L3**) and from δ = 109.1 ppm (**B**[14]) to δ = 114.9 (**L2**) and δ = 115.0 ppm (**L3**). Amide formation is also evident from the IR spectra of **L1**−**L3**; i.e., absorptions of the characteristic amide I and II vibrations[90] are found around $\tilde{\nu}$ = 1685/1689 cm^{-1} and $\tilde{\nu}$ = 1525/1531 cm^{-1}.

The π−π^* transitions of the metallo ligands **L1**−**L3** are observed around λ_{max} = 280 and 310 nm, and the characteristic ^{1}MLCT absorption bands are found in the visible spectral region (Table 1, Figure 1). As expected, the MLCT absorption of amino substituted **L1** appears at lower energy (λ_{max} = 500 nm) than those of **L2** and **L3** (λ_{max} = 492/493 nm) due to the electron donating effect of the amino group.[14,15] This electron donation raises the energy of one of the occupied ruthenium centered "t_{2g}" orbitals in **L1**, while the LUMO (located at the tpy-CO-R ligand) remains essentially constant in energy. At room temperature, the emitting ^{3}MLCT state of **L1** (λ_{em} = 727 nm) is also lower in energy than the emitting states of **L2** and **L3** (λ_{em} = 674/673 nm) due to the electron donating NH_2 group (Table 1). With respect to the parent compounds **A** and **B**, the quantum yields Φ = (15.0−16.6) × 10^{-4} of the metallo ligands are slightly lower, which could be due to the enhanced possibility of radiationless deactivation via high energy bipyridine CH vibrations.[91−94] The electron donating character of the NH_2 group also facilitates oxidation of Ru^{II} to Ru^{III} in **L1** as compared to **L2** and **L3** by more than 0.22 V. Several ligand centered reductions (tpy and bpy) are found between −1.48 and −2.49 V. However, assignment of the reduction processes to individual ligands from these data is difficult (Table 2).

Metallo ligand **L2** crystallized as acetonitrile solvate in the triclinic space group $P\bar{1}$ as ruby red crystals (Figure 2, Table S1 including a thermal ellipsoid plot). The metrics of the RuN_6 polyhedron are in a typical range for bis(terpyridine) ruthenium(II) complexes of this kind (Ru−N = 1.971−2.077 Å; N−Ru−N = 78.2−79.3°).[14] As expected, the 2,2′-bipyridine substituent is oriented in an *s-transoid* conformation (N8−C39−C40−N9 torsion angle = −178.4(3)°). One hexafluorophosphate counterion (P2) is hydrogen bonded to the amide NH group (N7···F7 = 3.307(3) Å) giving a contact ion pair while the other counterion (P1) is not engaged in hydrogen bonding (Figure 2, Table S1 including a thermal ellipsoid plot).

Single crystals of the constitutional isomer **L3** crystallized from a $[NH_4][PF_6]/H_2O/CH_3CN$ mixture as bipyridinium hexafluorophosphate salt **L3·HPF$_6$·2H$_2$O** with two water solvate molecules in the triclinic space group $P\bar{1}$ as ruby red crystals (Figure 3, Table S1 including a thermal ellipsoid plot). Bond distances and angles of the bis(terpyridine) ruthenium(II) core (Ru−N = 1.978−2.071 Å; N−Ru−N = 78.6−79.3°) are in the expected range.[14] Due to the electron withdrawing nature of the COR substituent at the inner pyridine ring of the

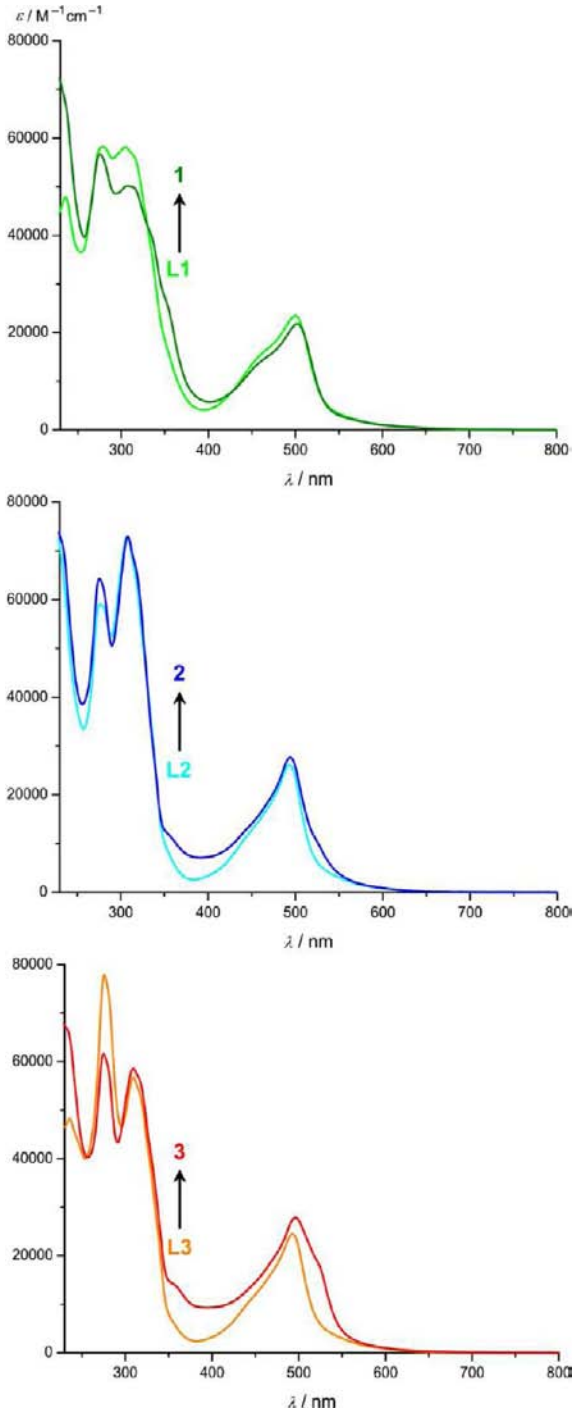

Figure 1. Electronic spectra of metallo ligands **L1**−**L3** and bimetallic complexes **1**−**3** in CH_3CN.

2,2′-bpy, the bpy is protonated at the remote more electron-rich pyridine ring (N9−H1). The additional positive charge is compensated by a further hexafluorophosphate counterion. The protonation results in an s-*cisoid* conformation of the 2,2′-bipyridine moiety (torsion angle N8−C39−C40−N9 = −12.8(5)°) instead of the preferred s-*transoid* conformation of pristine 2,2′-bipyridine. The amide units of **L3** are connected via hydrogen bonds with two water molecules (H2−O4−H3 and H4−O5−H5) along the crystallographic *a* axis (Figure 3, top). Protonated bpy units of an adjacent chain of complexes are attached to this water/amide chain via N9−H1···O4

dx.doi.org/10.1021/ic301632y | *Inorg. Chem.* 2013, 52, 1248−1264

Table 2. Redox Potentials (E/V vs. Fc/Fc^+) of L1−L3 and 1−3 in $CH_3CN/[nBu_4N][PF_6]$ at Room Temperature

	$Ru^{II/III}$	$Re^{I/II}$	$[ligand]^{0/-}$
L1	0.675		−1.525, −1.920,[a] −2.180,[a] −2.490[a]
L2	0.900		−1.480, −1.755,[a] −2.085, −2.330
L3	0.915		−1.565, −1.850,[a] −2.075, −2.325
1	0.685, 1.686 (NH_2[a])	0.980[a]	−1.465, −1.742,[a] −2.255,[a] −2.485[a]
2	0.910	0.985[a]	−1.480, −1.995, −2.125, −2.355
3	0.915	0.980[a]	−1.525, −1.975, −2.115, −2.360

[a]Irreversible, E_p given.

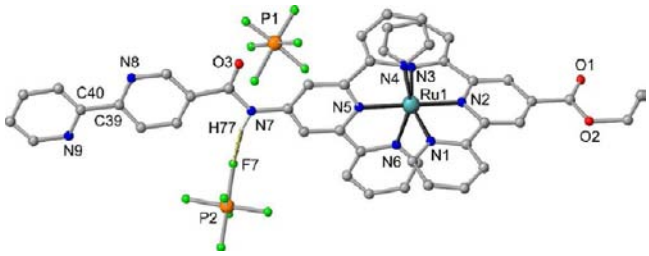

Figure 2. Molecular structure of **L2** in the solid state (CH hydrogen atoms omitted).

hydrogen bonds (Figure 3, top) giving a protonated water dimer (Zundel cation, $(H_5O_2)^+$) sandwiched between two amide units and a bipyridine moiety. The bpy moieties of adjacent chains stack onto each other in a centrosymmetric fashion with a center-to-center distance of the stacked pyridine rings of 3.8 Å. Furthermore, two $[PF_6]^-$ counterions (P2, P3) are attached to the chain by P2−F8···H3 and P3−F15···H4 hydrogen bonds (Figure 3, bottom). The third $[PF_6]^-$ ion (P1) is not involved in this supramolecular arrangement. It is stressed at this point that coordination of solvent molecules or counterions to positively charged amide units appears to be a general phenomenon but has not been considered in detail with respect to weakly coordinating anions. Binding of stronger coordinating anions like $H_2PO_4^-$ or halides to amides has been investigated in detail for example by Beer and co-workers.[95]

The assembly of the ions in the solid state of **L2** can be viewed as a snapshot of an intimate contact ion pair (Figure 2) while the supramolecular arrangement of **L3·HPF$_6$·2H$_2$O** can be described as a snapshot of a solvent-separated ion pair including parts of the solvent shell (Figure 3, bottom). DFT (B3LYP, LANL2DZ) geometry optimizations including solvent modeling (IEFPCM, CH_3CN) were performed for the dications of **L1−L3** (Figure S1). As expected, the *s-transoid* conformation of the 2,2′-bipyridine moiety is preferred in unprotonated bipyridine derivatives. At the bridging amide unit, the oligopyridine ligands are slightly out of plane with the torsion angles between the tpy, bpy, and amide units ranging from 1 to 27°, which is in accordance with the X-ray data from **L2** and **L3·HPF$_6$·2H$_2$O**.

The three highest occupied molecular orbitals of **L1−L3** are essentially centered on ruthenium with the HOMO of **L1** also being delocalized onto the NH_2 group (see Figure S2 for a graphical representation of the relevant Kohn−Sham molecular orbitals).[14,15] In all cases, the LUMO is delocalized over the CO substituted tpy ligand, i.e., toward the bpy in the case of **L1** and in the opposite direction for **L2** and **L3**. This MO description translates into a ruthenium based oxidation and a tpy-CO based reduction. In fact, spin densities calculated for the one-electron oxidized species $[\mathbf{L1}]^+$−$[\mathbf{L3}]^+$ (see Figure S3 for a graphical representation) are essentially localized on ruthenium with a contribution of the NH_2 group in the case of $[\mathbf{L1}]^+$ similar to results obtained for amino acid **A**.[14,25] The spin densities of the one-electron reduced species $[\mathbf{L1}]^-$−$[\mathbf{L3}]^-$ are distributed over the central pyridine ring and the carbonyl group of the CO-substituted tpy ligand and to some extent over the ruthenium center (see Figure S3 for a graphical representation). Thus, the oxidation is assigned to the $Ru^{II/III}$ couple, and the first reduction is basically assigned to the reduction of the tpy-CO ligand with some Ru admixture (Table 2).

L1−L3 were chemically reduced using decamethylcobaltocene (E = −1.91 V vs Fc/Fc^+[96]) or an excess cobaltocene ($E \approx$ −1.33 V vs Fc/Fc^+[96]) in acetonitrile. During reduction characteristic changes of absorption bands are observed in the corresponding electronic spectra (Figure 4). In all cases, a new band around 350 nm arises. For $[\mathbf{L2}]^-$ and $[\mathbf{L3}]^-$, the original MLCT band of **L2** and **L3** is shifted to lower energy (516 nm) with an isosbestic point at 500 nm, while a broadening of the MLCT band of **1** is noted for $[\mathbf{L1}]^-$. As in fluid solution no EPR signals were obtained, rapid-freeze EPR spectroscopy was undertaken with the hope to acquire meaningful EPR spectra at 77 K. Indeed, for $[\mathbf{L2}]^-$ and $[\mathbf{L3}]^-$ rhombic signals were obtained at 77 K ($g_{1,2,3}$ = 2.0102, 1.9939, 1.9712; Δg = 0.0390 and $g_{1,2,3}$ = 2.0095, 1.9935, 1.9709; Δg = 0.0386 by spectral simulation; peak-to-peak distances 64 and 59 G) giving g_{iso} = 1.9918 and 1.9914 for $[\mathbf{L2}]^-$ and $[\mathbf{L3}]^-$, respectively (Figure 5 and Figure S4). These values are in good agreement with those observed for $[Ru(tpy)_2]^+$ ($g_{1,2,3}$ = 1.991, 1.991, 1.960;[97] Δg = 0.031; g_{iso} = 1.986[98]) suggesting some ruthenium d-orbital admixture in the redox orbital which is supported by the DFT calculations on $[\mathbf{L2}]^-$ and $[\mathbf{L3}]^-$ (Figure 5 and Figure S3).

Using CAN (ceric ammonium nitrate; $E \approx$ 1.3 V vs Fc/Fc^+[96]) in the acidic medium oxidation of **L1** to $[\mathbf{L1}]^+$ is successful. The EPR spectrum of $[\mathbf{L1}]^+$ ($g_{1,2,3}$ = 2.347, 2.185, 1.857; Δg = 0.490; g_{iso} = 2.139; Figure S5) at 77 K is very similar to that of $[\mathbf{B}]^+$ ($g_{1,2,3}$ = 2.347, 2.178, 1.843; Δg = 0.504; g_{iso} = 2.133; Figure S5) showing a characteristic Ru^{III} signature modulated by partial delocalization of spin density onto the ligand (tpy-NH_2).[99−101] The described EPR experiments confirm that reduction occurs at tpy-CO plus some Ru while oxidation occurs at Ru plus some tpy-NH_2.

According to DFT calculations, the lowest energy triplet states of **L1−L3** correspond to ^{3}MLCT states involving the tpy-CO ligand as an acceptor and ruthenium as a donor, which fits to the corresponding one-electron reduced and one-electron oxidized species (see Figure S3 for graphical descriptions of the spin densities). For $^3[\mathbf{L1}]$, some admixture of the peripheral tpy-NH_2 ligand to the donor part is also involved.[15] This is also in accordance with the observed bathochromic emission shift of **L1** as compared to **L2** and **L3** (Table 1). Having assigned relevant basic spectral and redox characteristics in the metallo ligands **L1−L3**, we now focus on the heterobimetallic systems **1−3**.

Complexation of Metallo Ligands L1−L3 and Properties of Ru~Re Complexes 1−3. Metalation of the bpy ligands **L1−L3** with $ReCl(CO)_5$ results in the desired *fac*-tricarbonyl chloro rhenium(I) derivatives **1−3** in good to excellent yields (see Experimental Section, Scheme 2).

The successful installation of the $Re^ICl(CO)_3$ fragment is confirmed by observing peaks for the molecular ions $[M+PF_6]^+$

dx.doi.org/10.1021/ic301632y | Inorg. Chem. 2013, 52, 1248−1264

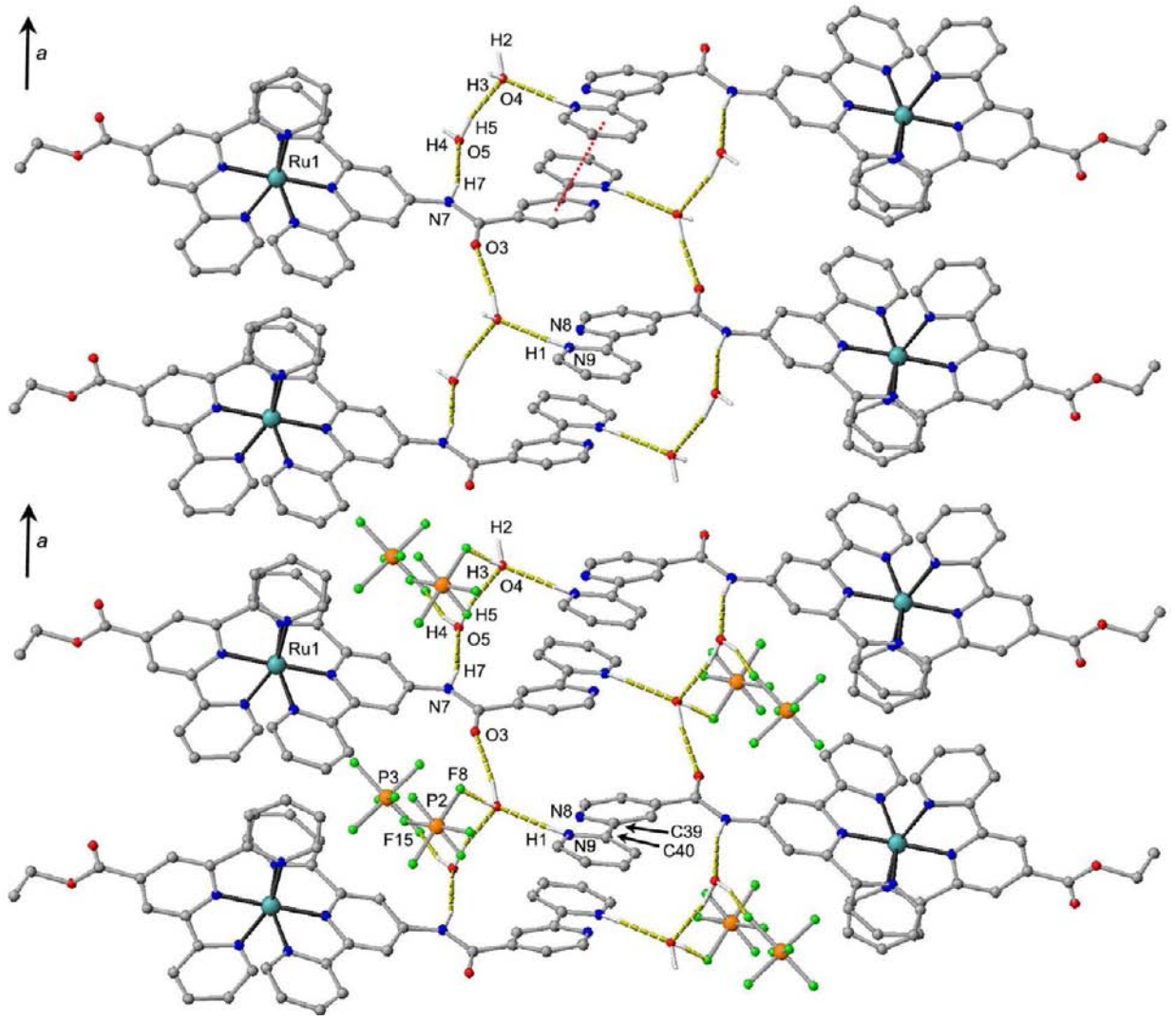

Figure 3. Intermolecular hydrogen bond network of **L3·HPF$_6$·2H$_2$O** in the solid state (only hydrogen bonds with D−H···A angles >130° are shown). Top: hydrogen bonded chains without counterions, the bpy stacking is indicated by a red dotted line. Bottom: chains with two counterions (P2, P3) attached (CH hydrogen atoms and counterion P1 omitted).

of **1**−**3** in the corresponding ESI mass spectra. Significant coordination shifts are found for proton resonances H^9, H$^{10/11}$, and H^{18} and most carbon resonances of the bpy unit, while the terpyridine resonances remain essentially unaffected. However, for the pair **L3**/**3** more proton resonances are significantly shifted to lower field, namely those of H$^{2'}$, H$^{5'}$, H^{10}, H^{12}, H^{15} ($\Delta\delta$ = 0.35 − 0.71 ppm), and NH ($\Delta\delta$ = 2.28 ppm). The schematic drawing of **3** (Scheme 2) suggests that exactly these protons establish binding pockets to which a hexafluorophosphate counterion can coordinate via NH···F and CH···F hydrogen bonds.

Indeed, DFT (B3LYP, LANL2DZ, IEFPCM) geometry optimizations on the dication of **3** with an explicit $[PF_6]^-$ counterion attached to the NH group find these protons establishing H···F contacts below 2.5 Å. Binding pockets are formed in two different conformations **3$_a$** and **3$_b$** (Figure 6). Obviously, hexafluorophosphate is a quite strongly coordinating anion toward amide units flanked by positively charged units,[68,74] which has also been exemplified in the solid state of **L2**. Hence the NMR study suggests significant ion pairing for **3** also *in solution*—especially to conformer **3$_a$**—which is not only a dynamic electrostatic attachment[102] but largely driven by hydrogen bonding.

In all cases **1**−**3**, the characteristic infrared signature of the ReCl(CO)$_3$(bpy) units is found in the range $\tilde{\nu}$ = 1900−2023 cm^{-1} in acetonitrile.[32] The CO stretching vibrations of the *N*-substituted bpy derivative **1** ($\tilde{\nu}$ = 2022, 1915, 1900 cm^{-1}) occur at slightly lower energy as compared to those of the CO-substituted bpy complexes **2** and **3** ($\tilde{\nu}$ = 2023, 1919, 1902 cm^{-1}), which is in line with the expected electron donating/withdrawing capability of the different bpy ligands. This electronic modulation subsequently modifies the π-back-donation of the rhenium center to the carbonyl ligands. DFT calculations (B3LYP, LANL2DZ, IEFPCM) on **1**−**3** and harmonic frequency calculations indeed reproduce this weakly pronounced hypsochromic trend for **1** → **2**/**3** ($\Delta\tilde{\nu}$ = 1 − 4 cm^{-1}). In acetonitrile solution **1** displays two further weak $\tilde{\nu}$(CO) absorption bands at $\tilde{\nu}$ = 2035 and $\tilde{\nu}$ = 1932 cm^{-1}. By comparison with $[Re(bpy)(CH_3CN)(CO)_3]^+$ ($\tilde{\nu}$(CO) = 2041, 1937 cm^{-1}[140]) these bands can be assigned to species **1**′ obtained from chloride substitution by acetonitrile at the Re site. The higher lability of chloride in **1** as compared to **2** and **3**

dx.doi.org/10.1021/ic301632y | Inorg. Chem. 2013, 52, 1248−1264

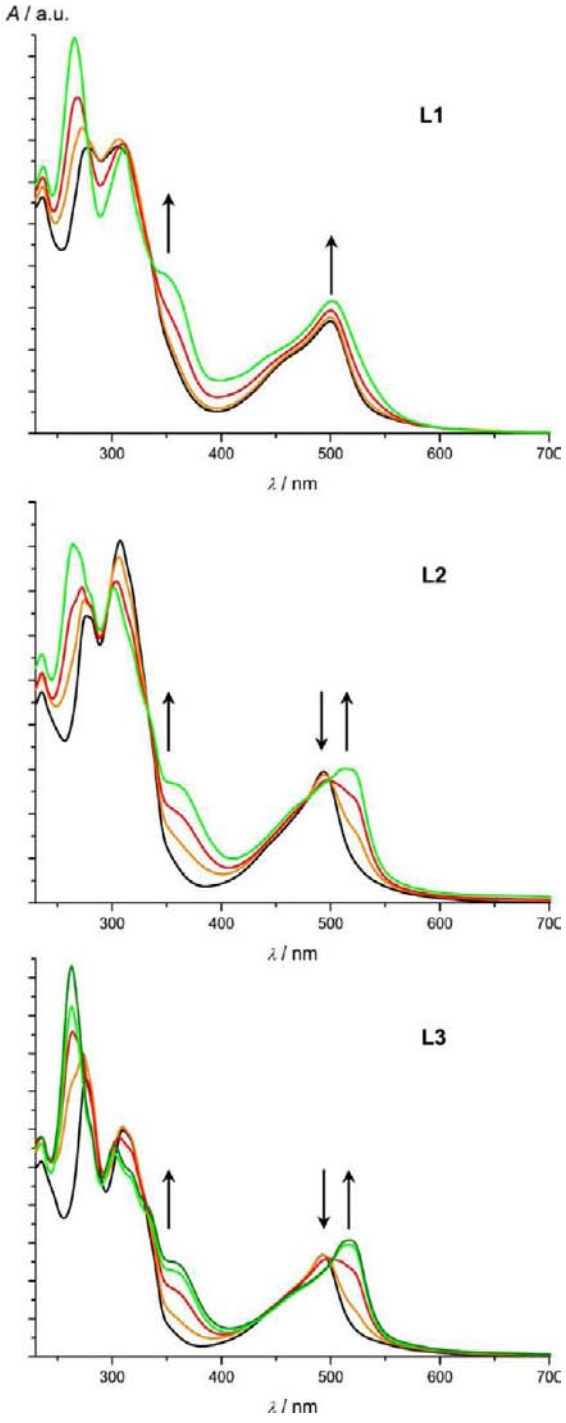

Figure 4. Electronic spectra of **L1**−**L3** in CH_3CN during reduction.

is based on the more electron donating character of the *N*-substituted bpy ligand in **1**.

Coordination of the rhenium carbonyl fragment to the metallo ligands **L1**−**L3** slightly shifts the $Ru^{II} \rightarrow$ tpy ^{1}MLCT absorption bands bathochromically by ∼100 cm^{-1} (Figure 1, Table 1). The $Re^{I} \rightarrow$ bpy ^{1}MLCT absorptions are found as weak shoulders at λ_{max} = 353 nm (**1**), 367 nm (**2**), and 362 nm (**3**) (Figure 1; λ_{max} values are obtained from the difference spectra **1**−**L1**, **2**−**L2**, and **3**−**L3**) in accordance with the trend observed for reported mononuclear 4,4′-disubstituted bpy complexes $ReCl(CO)_3[4,4'\text{-}(NHCOCH_3)_2bpy]$ (λ_{max} = 364 nm) and $ReCl(CO)_3[4,4'\text{-}(COOEt)_2bpy]$ (λ_{max} = 412 nm).[32]

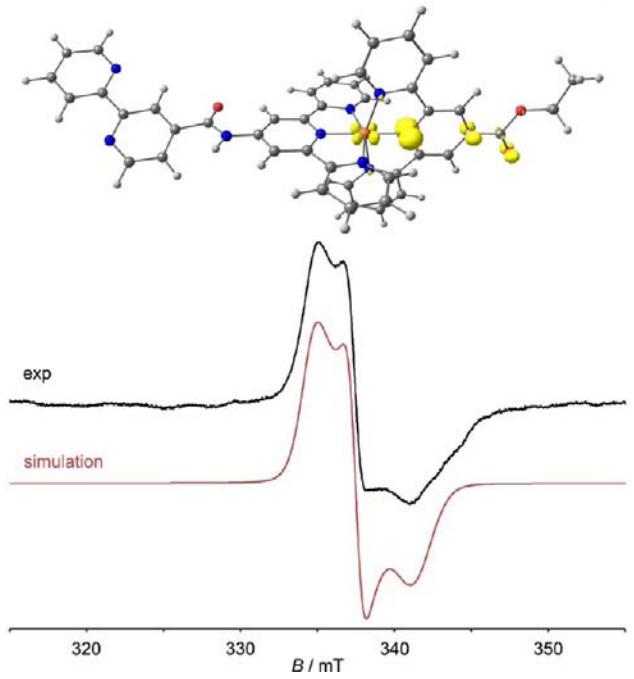

Figure 5. Spin density plot of $[\mathbf{L3}]^-$ (top, isosurface value 0.01 au) and X-band EPR spectrum of $[\mathbf{L3}]^-$ (bottom) at 77 K in CH_3CN (9.42 GHz) and simulation (in red).

In the mixed-metal complexes **1**−**3**, room temperature emission from the ^{3}MLCT(Ru) and ^{3}MLCT(Re) states is expected to lie at comparable energies due to the typically large apparent Stokes shift of the Re based emission.[32] The room temperature emission spectra of the metallo ligands **L1**−**L3** and the heterobinuclear complexes **1**−**3** are very similar within the limits of our instrumentation (Figure 7). We note a slightly higher emission intensity when exciting in the region of the MLCT(Re) absorption band (λ_{exc} < 410 nm) in **1**−**3** as compared to **L1**−**L3** (Figure 7) with matched absorptions at the ^{1}MLCT(Ru) maximum due to the larger extinction coefficient of **1**−**3** in that spectral region ($Re^I \rightarrow$ bpy ^{1}MLCT). We propose either that the Re based emission indeed occurs at a very similar energy and with a very similar band shape or—as a more likely scenario—that the energy is transferred from ^{3}MLCT(Re) to ^{3}MLCT(Ru) at λ_{exc} < 410 nm, as is typically observed for Ru∼Re complexes.[103−106] Both Förster and Dexter type energy transfer mechanisms have been discussed in this context. A Dexter type mechanism is also conceivable for the conjugated bpy−amide−tpy bridge of **1**−**3**.

At 77 K in a butyronitrile matrix, the emission bands are better resolved and feature vibrational fine structure (Figure 8). Again, exciting the MLCT(Re) of **1**−**3** at λ_{exc} < 410 nm results in a stronger emission as compared to that of **L1**−**L3**, and we suggest an energy transfer from Re to Ru. Notably, the shapes of the emission bands of **1** and **L1** are different, the emission bands of **1** being broader than those of **L1** (Figure 8, left). This could be due to emission from **1** and from its rhenium solvento complex **1′** already detected by IR spectroscopy (vide supra). The Ru based emission from the solvento complex **1′** bearing a positively charged electron withdrawing (bpy)Re site should indeed occur at lower energy than the emission of **1**.

In order to gain more insight into the nature of the low-energy triplet states of **1**−**3**, DFT calculations (B3LYP, LANL2DZ, IEFPCM) were performed (Figure 9). The low

dx.doi.org/10.1021/ic301632y | Inorg. Chem. 2013, 52, 1248−1264

Scheme 2. Synthesis of Ruthenium−Rhenium Conjugates 1−3 and Atom Numbering Used for NMR Assignments

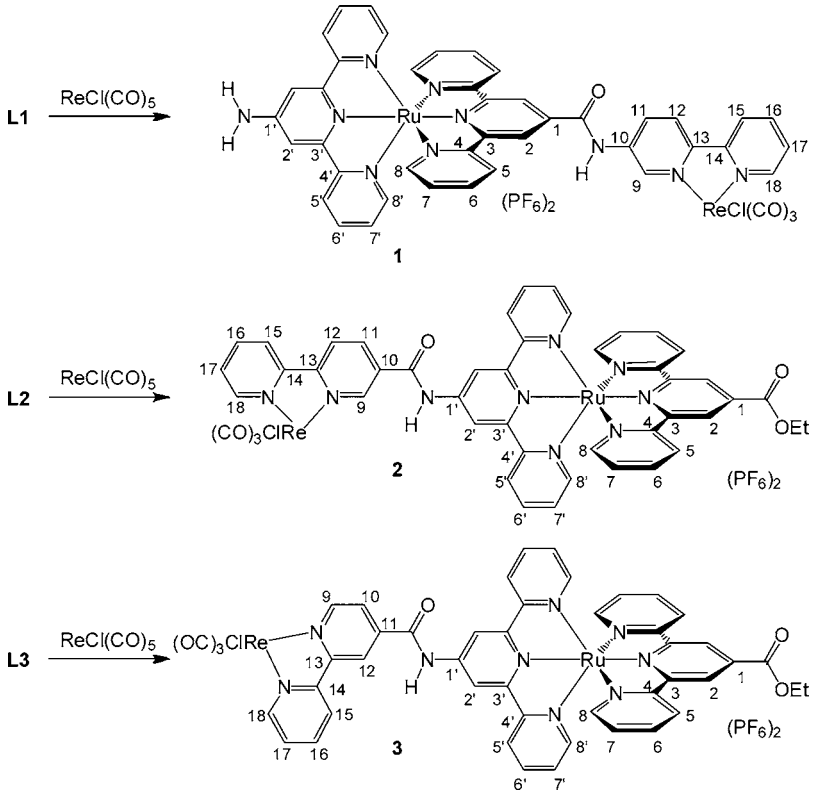

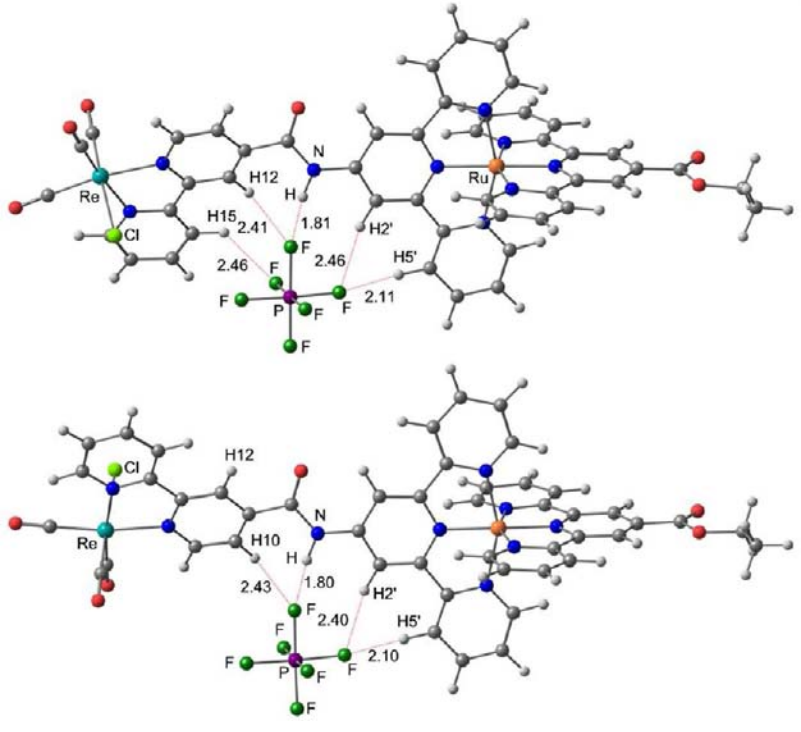

Figure 6. Suggested ion paring of the dication of **3** with $[PF_6]^-$ in acetonitrile in different conformations $\mathbf{3}_a$ (top) and $\mathbf{3}_b$ (bottom); DFT (B3LYP, LANL2DZ, IEFPCM) optimized geometries; F···H distances given in Å.

energy ^{3}MLCT states of $^3[\mathbf{L1}]$–$^3[\mathbf{L3}]$ and $^3[\mathbf{1}]$ (in its two isoenergetic conformations $^3[\mathbf{1}_a]$ and $^3[\mathbf{1}_b]$) are localized on ruthenium and on the tpy-CO unit as expected (Figure S3 and Figure 9; Mulliken spin density at Ru = 0.85). For the linear Ru∼Re derivative $^3[\mathbf{2}]$ (4-CO substituted bpy), the two conformations $^3[\mathbf{2}_a]$ and $^3[\mathbf{2}_b]$ lead to two distinct ^{3}MLCT-(Ru) states centered either on the terminal (conformer $^3[\mathbf{2}_a]$; Mulliken spin density at Ru = 0.90) or on the bridging tpy ligand (conformer $^3[\mathbf{2}_b]$; Mulliken spin density at Ru = 0.80; calculated slightly higher in energy by 11 kJ mol^{-1}). On the

dx.doi.org/10.1021/ic301632y | Inorg. Chem. 2013, 52, 1248−1264

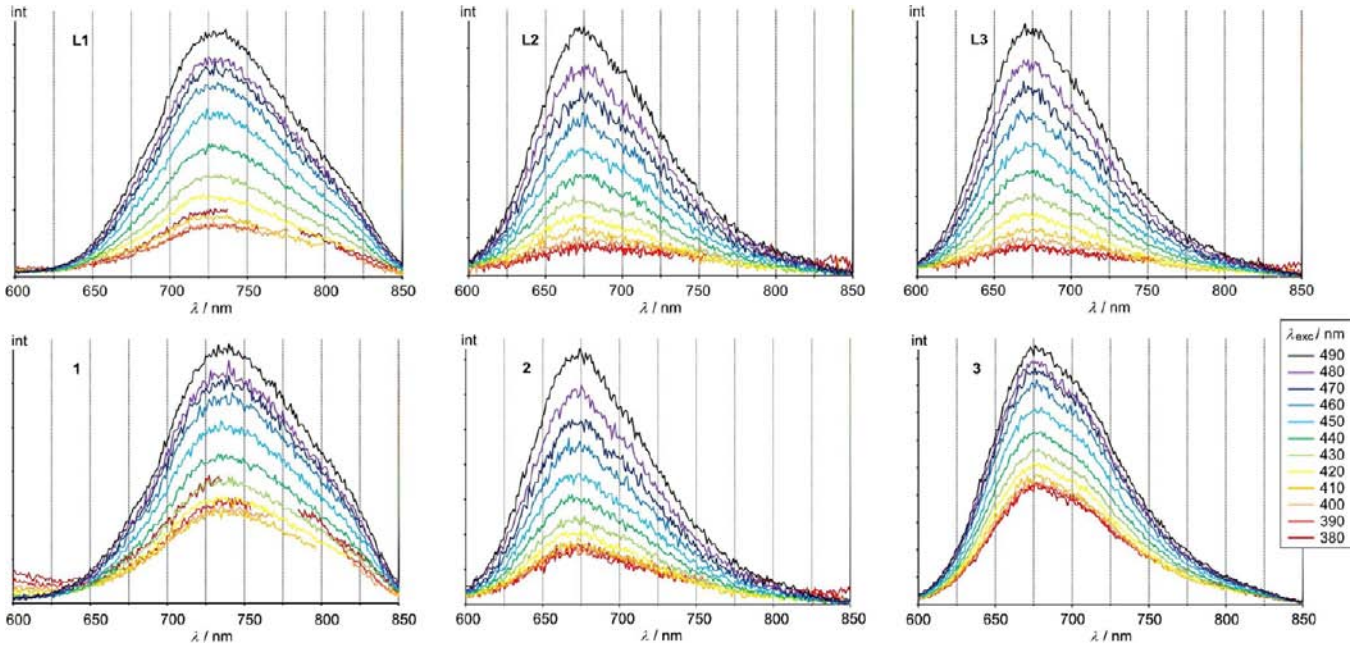

Figure 7. Emission spectra of **L1**−**L3** (top) and **1**−**3** (bottom) at 300 K in deaerated CH_3CN with varying excitation energy.

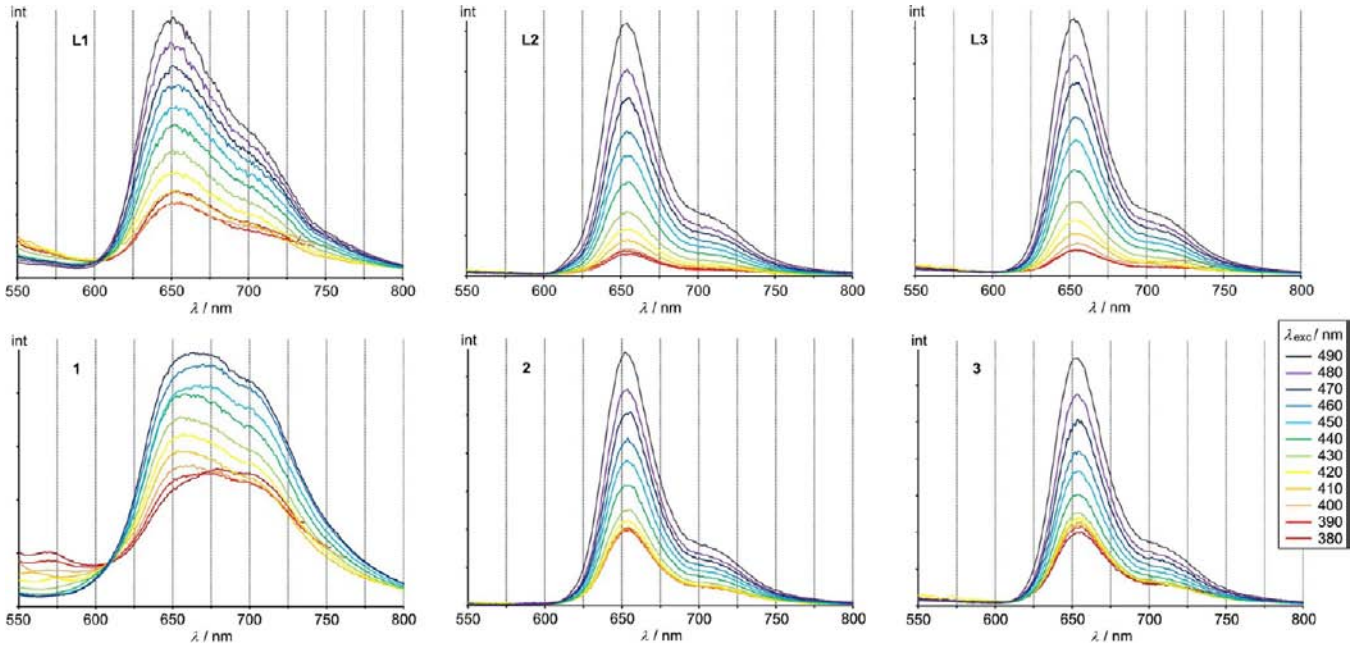

Figure 8. Emission spectra of **L1**−**L3** (top) and **1**−**3** (bottom) at 77 K in a butyronitrile matrix with varying excitation energy.

other hand, both conformers $^3[\mathbf{3}_a]$ and $^3[\mathbf{3}_b]$ of the 5-CO substituted bpy derivative feature low-energy Re(bpy) based ^{3}MLCT states (Mulliken spin density at Re = 0.61), which is clearly at odds with the experiment. Obviously, the DFT calculations suggest a subtle energetic balance between the different ^{3}MLCT states depending on the type of substituent (CONH, NHCO) and its position at the bpy ligand. Furthermore, we suggest that ion pairing also manipulates the relative excited state energies by coordination of anions to NH groups.[107] Of course, these phenomena are not reflected in the continuum model used for the calculations. Thus, we performed calculations on $^3[\mathbf{3}_{a/b}]$ including an explicit counterion attached to the amide bridge. Indeed, anion binding shifts the spin density back to the tpy-CO ligand which is now in full accord with the experiments (Figure 9, bottom). From the experimental and theoretical data we suggest that ^{3}MLCT-(Ru) and ^{3}MLCT(Re) states of $^3[\mathbf{3}]$ are very close in energy and that their relative energy and relative population (excited state equilibration) is modulated by the coordination of counterions to the amide unit. Such a coordination has indeed been suggested for **3** on the basis of the NMR data (vide supra). Given that this anion binding is present in $\mathbf{3}_{a/b}$ and in $^3[\mathbf{3}_{a/b}]$ we propose that emission observed for **1**−**3** originates essentially from the lowest energy ^{3}MLCT(Ru/tpy-CO) state (Figure 10).

The electrochemical features of **1**−**3** are basically similar to those of **L1**−**L3** with an additional irreversible oxidation wave observed at nearly 1 V which is assigned to the $Re^{I/II}$ couple

dx.doi.org/10.1021/ic301632y | Inorg. Chem. 2013, 52, 1248−1264

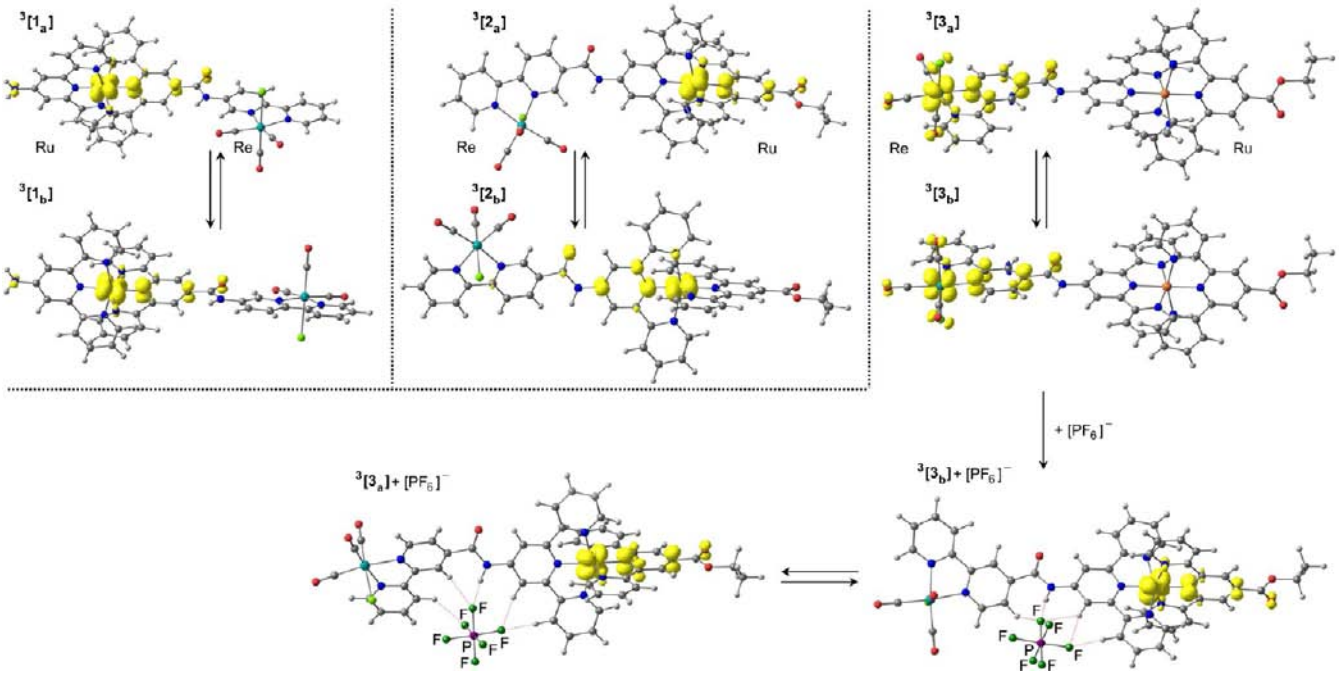

Figure 9. DFT (B3LYP, LANL2DZ, IEFPCM) calculated spin densities of $^3[\mathbf{1}_{a/b}]$, $^3[\mathbf{2}_{a/b}]$, and $^3[\mathbf{3}_{a/b}]$ in two conformations a/b and with explicit inclusion of a $[PF_6]^-$ counterion for $^3[\mathbf{3}_{a/b}]$ (isosurface value 0.01 au).

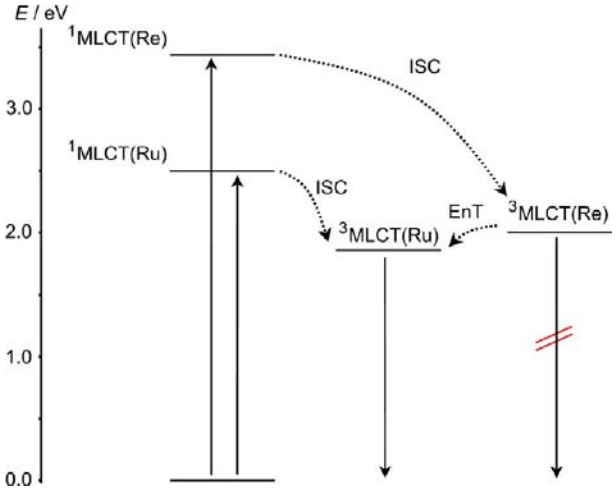

Figure 10. Qualitative energy diagram for **1**–**3** (ISC = intersystem crossing; EnT = energy transfer).

(Table 2). For the $[(4,4'\text{-}Me_2bpy)_2Ru\text{-(linker)-}ReCl(4,4'\text{-}Me_2bpy)(CO)_3]^{2+}$ binuclear complexes reported by Ishitani, the Ru^{II} moiety is also easier to oxidize than the Re^{I} fragment.[51,52] Similar to **L1**–**L3**, several reduction processes are observed for **1**–**3** and assigned to ligand-based reductions (Table 2).

CAN in an acidic medium oxidizes **1** to $[\mathbf{1}]^+$, and characteristic optical responses are noted, namely the decline of the MLCT(Ru) absorption band at 502 nm and the growth of the corresponding LMCT(Ru) absorption band at 725 nm with an isosbestic point at 584 nm (Figure S6). These observations are in full agreement with the previously reported behavior of the $\mathbf{A}/[\mathbf{A}]^+$ redox pair.[25] The EPR spectrum of $[\mathbf{1}]^+$ in frozen acetonitrile gives an anisotropic signal pattern with $g_{1,2,3}$ = 2.349, 2.184, 1.850 (Δg = 0.499; g_{iso} = 2.138) similar to $[\mathbf{L1}]^+$ and $[\mathbf{B}]^+$ (vide supra, Figure S5). DFT calculations also support a $Ru^{II/III}$ based redox process (with some participation of the NH_2 group) for the $\mathbf{1}/[\mathbf{1}]^+$ redox couple (Figure 11). Using time-dependent DFT calculations (B3LYP, LANL2DZ, IEFPCM) on $[\mathbf{1}]^+$, the band at 725 nm ($\lambda_{max,calcd}$ = 684 nm, f = 0.1831) is assigned to a ligand-to-metal charge transfer localized at the terminal Ru/tpy-NH_2 site (Figure S6). Redox potentials and DFT calculations suggest that the one-electron oxidation of **2** and **3** also occurs at the Ru center, although preparative oxidation with CAN is unsuccessful due to its too low oxidation potential (Table 2, Figure 11).

The site of the one-electron reduction is much more challenging to assign, which is similar to the difficult assignment of the lowest ^{3}MLCT state (Figures 9 and 11). The experimental electronic spectra of the one-electron reduced Ru~Re species $[\mathbf{1}]^-$–$[\mathbf{3}]^-$ are similar to those of the corresponding reduced metallo ligands $[\mathbf{L1}]^-$–$[\mathbf{L3}]^-$. This suggests that under these conditions the odd electron occupies a molecular orbital associated with the ruthenium site, namely the tpy-CO ligand in all cases (vide supra and Figure S7).

To spectroscopically probe the Re(bpy) component of $[\mathbf{1}]^-$–$[\mathbf{3}]^-$, solution IR spectra in the characteristic $\tilde{\nu}$(CO) region were acquired during one-electron reduction of **1**–**3** by cobaltocene or decamethyl cobaltocene. Typically, reduction of $ReCl(bpy^R)(CO)_3$ complexes to $[ReCl(bpy^R)(CO)_3]^-$ results in large bathochromic shifts ($\Delta\tilde{\nu}$ = 20–30 cm^{-1}) of the CO stretching vibrations due to the stronger π-back-donating ability of the $[Re^I(bpy^-)]$ unit toward the carbonyl ligands.[40] For **1**–**3** treated with $CoCp_2$, only marginal bathochromic shifts in the range of $\Delta\tilde{\nu}$ = 1 – 6 cm^{-1} are recorded (Figure S8), suggesting that the odd electron indeed localizes in the vicinity of ruthenium (i.e., on tpy) and not on the rhenium coordinated bpy under these conditions. Upon reducing **1**–**3** with two equivalents of the stronger reducing reagent decamethylcobaltocene,[96] four additional absorption bands grow (**1** + 2$CoCp^*_2$: $\tilde{\nu}$ = 1983, 1948, 1882, 1847 cm^{-1}; **2** + 2$CoCp^*_2$: $\tilde{\nu}$ = 1983, 1946, 1883, 1850 cm^{-1}; **3** + 2$CoCp^*_2$: $\tilde{\nu}$ = 1983, 1948,

dx.doi.org/10.1021/ic301632y | Inorg. Chem. 2013, 52, 1248–1264

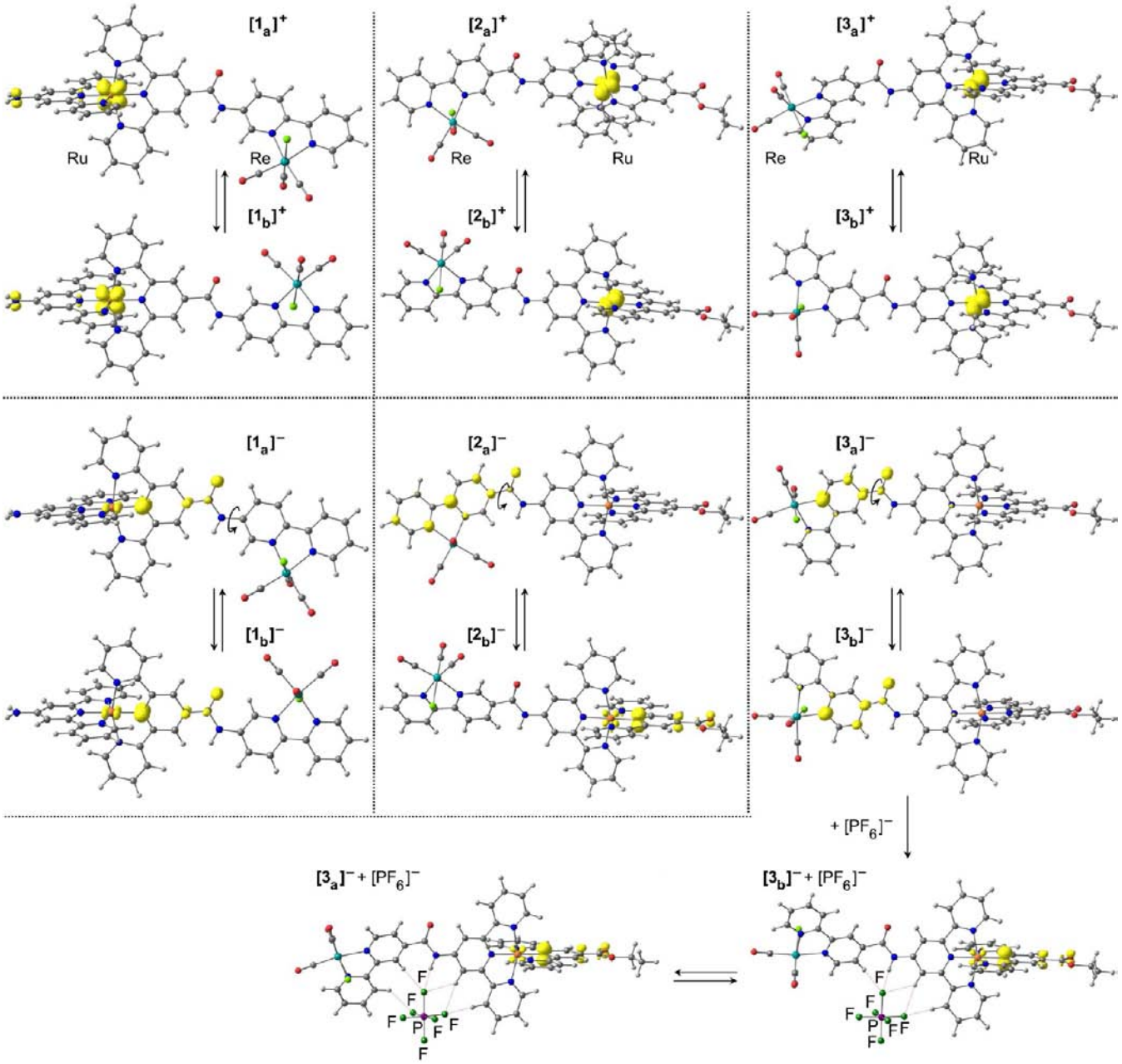

Figure 11. Spin densities of $[\mathbf{1}_{a/b}]^+$, $[\mathbf{2}_{a/b}]^+$, and $[\mathbf{3}_{a/b}]^+$ and $[\mathbf{1}_{a/b}]^-$, $[\mathbf{2}_{a/b}]^-$, and $[\mathbf{3}_{a/b}]^-$ (in different conformations a/b) obtained from DFT calculations (B3LYP, LANL2DZ, IEFPCM) and with explicit inclusion of a $[PF_6]^-$ counterion for $[\mathbf{3}_{a/b}]^-$ (isosurface value 0.01 au).

1883, 1850 cm^{-1}) at the expense of the original absorption bands. For the latter case, the original $\tilde{\nu}$(CO) bands even vanish completely. The new absorption bands can be assigned to dimerized 17 valence electron Re^0 species $[Re(\mathbf{L1})(CO)_3]_2^{n+}$, $[Re(\mathbf{L2})(CO)_3]_2^{n+}$, and $[Re(\mathbf{L3})(CO)_3]_2^{n+}$ by comparison of the IR patterns with those of $[Re(bpy)(CO)_3]_2$ ($\tilde{\nu}$ = 1986, 1950, 1888, 1857 cm^{-1}[140]) and $[Re(4,4'\text{-}Me_2bpy)(CO)_3]_2$ ($\tilde{\nu}$ = 1982, 1943, 1876, 1843 cm^{-1}[143]). Thus, we conclude that the first reduction is centered on the tpy-CO ligand, while the second reduction is located at the bpy ligand. The two-electron reduction induces chloride dissociation and dimerization in accordance with the irreversibility of the second reductive CV wave and literature precedence (Table 2).[40,43] Thus, both UV/vis and IR spectroscopy corroborate that the first site of reduction is located on the tpy-CO ligand in **1**−**3** in solution at room temperature.

A different situation is encountered in frozen solution. Rapid-freeze EPR spectra were acquired for $[\mathbf{1}]^-$−$[\mathbf{3}]^-$ (Figure 12 and Figure S9). At 77 K, one-electron reduced **1** displays a typical slightly anisotropic Ru^{II}/radical pattern ($g_{1,2,3}$ = 2.0175, 1.9979, 1.9800; Δg = 0.0375 by spectral simulation; peak-to-peak distance 48 G; g_{iso} = 1.9985) similar to that of $[\mathbf{L2}]^-$ and $[\mathbf{L3}]^-$.[97,98] This result fits to the DFT calculated spin density of $[\mathbf{1}]^-$ being concentrated on the central pyridine ring of the tpy-CO ligand and ruthenium (Figure 11, left). On the other hand, $[\mathbf{2}]^-$ and $[\mathbf{3}]^-$ show almost isotropic EPR resonances at g = 2.0108 ($[\mathbf{2}]^-$) and g = 2.0098 ($[\mathbf{3}]^-$) at 77 K and smaller peak-to-peak distances of 16 and 29 G, respectively (Figure 12 and Figure S9). These values are distinctly different from those of $[\mathbf{L2}]^-$ and $[\mathbf{L3}]^-$. As the radical $[ReCl(bpy)(CO)_3]^-$ also features a g_{iso} = 2.0032 resonance, the rapid-freeze EPR spectra of $[\mathbf{2}]^-$ and $[\mathbf{3}]^-$ are compatible with bpy-CO centered radicals

dx.doi.org/10.1021/ic301632y | Inorg. Chem. 2013, 52, 1248−1264

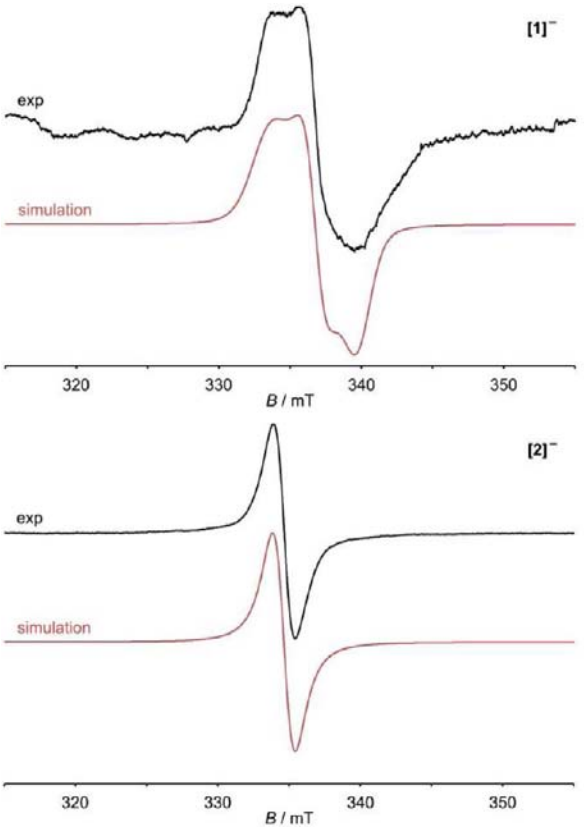

Figure 12. X-band EPR spectra of $[\mathbf{1}]^-$ (top) and $[\mathbf{2}]^-$ (bottom) at 77 K in CH_3CN (9.42 GHz) and simulation (in red).

coordinated to rhenium.[108−110] In frozen solution of $[\mathbf{2}]^-$ and $[\mathbf{3}]^-$, the odd electron localizes at bpy (EPR), while at room temperature the odd electron localizes at the tpy-CO ligand (UV, IR).

DFT calculations of $[\mathbf{2}]^-$ and $[\mathbf{3}]^-$ in different conformations a/b suggest bpy-CO centered radicals with the exception of the $[\mathbf{2_b}]^-$ conformer featuring a tpy-CO centered radical at the Ru terminus (Figure 11, middle). Both valence isomeric situations are obviously close in energy in $[\mathbf{2}]^-$ and $[\mathbf{3}]^-$ and influenced by the conformation a/b and probably also by coordination of the counterion (different ion paring in liquid and in frozen solution). Indeed, explicitly including a $[PF_6]^-$ counterion coordinated to the NH group of $[\mathbf{3}]^-$ in the DFT calculation shifts the spin density toward the tpy-CO ligand (Figure 11, bottom).

We checked this interpretation experimentally by exchanging the $[PF_6]^-$ counterion of **3** with $[BPh_4]^-$, which is unable to coordinate to the NH group. The successful ion exchange to **3*** was confirmed by ^{31}P and ^{19}F NMR spectroscopy. Gratifyingly, the rapid-freeze 77 K EPR spectrum of the corresponding one-electron reduced species $[\mathbf{3^*}]^-$ (generated by reduction of **3*** with $CoCp^*_2$) displays the expected pattern for the Ru^{II}/radical ($g_{1,2,3}$ = 2.0140, 1.9935, 1.9750; Δg = 0.0390 by spectral simulation; peak-to-peak distance 63 G; g_{iso} = 1.9942; Figure S9) in contrast to $[\mathbf{3}]^-$ showing the bpy radical. Furthermore, the IR spectrum of $[\mathbf{3^*}]^-$ features low-energy CO absorptions attributable to $[ReCl(\mathbf{L3})(CO)_3]^-$ ($\tilde{\nu}$ = 2006 cm^{-1}, Figure S8) which are subsequently replaced by absorptions assigned to the dimerized chloride-free species $[Re(\mathbf{L3})(CO)_3]_2^{n+}$ (vide supra). Thus, the valence isomeric equilibrium $[\mathbf{3^*}]^-/[\mathbf{3}]^-$ (Re/bpy radical vs Ru/tpy radical) is modulated by the type of counterions; in other words coordination of a counterion (effector) at the bridging amide unit shifts the spin density from the *N*- to the *C*-terminus of the ruthenium amino acid moiety. In addition to the charge shift in the one-electron reduced species $[\mathbf{3^*}]^-$ and $[\mathbf{3}]^-$, the emission band of **3*** experiences a slight hypsochromic shift from $\lambda_{em}(\mathbf{3})$ = 678 nm to $\lambda_{em}(\mathbf{3^*})$ = 671 nm, showing a higher energy of the ^{3}MLCT(Ru,**3***) state possibly approaching the ^{3}MLCT(Re,**3***) energy (Figure 9, Table 1, Figure S10). Furthermore, the emission intensity of **3*** upon excitation below λ_{exc} = 410 nm is much lower than that of **3**, suggesting a less efficient energy transfer from Re to Ru in **3***.

The feasibility of photoinduced electron transfer was probed by reductive quenching of the excited triplet states using triethanolamine (TEOA) as an electron donor. The estimated redox potentials of the ^{3}MLCT(Ru) excited states are around E = 0.33−0.42 V (Table 3, vs Fc/Fc^+) so that the excited complexes should be able to oxidize TEOA to its radical cation $[TEOA]^{\bullet+}$ (E = 0.82 V vs NHE; E = 0.19 V vs Fc/Fc^+[34,35]). Indeed, quenching experiments with TEOA lead to quenching fractions η_q = 0.09−0.99 (c_{TEOA} = 0.1 M) when exciting at 500 nm (Table 3). Using the reported life times of the ^{3}MLCT(Ru) states of **A**, **B**, or their known derivatives in CH_3CN of around τ = 21.7−33.7 ns,[14−16] the quenching rate constants span a range from $k_q = 3.9 \times 10^7$ to 3.5×10^{10} M^{-1} s^{-1} apparently uncorrelated to the thermodynamic driving force (Table 3). It is seen that quenching is more effective for the bimetallic complexes **1**−**3** as compared to the quenching of their constituting metallo ligands **L1**−**L3**, and efficiency increases in both series **L1** < **L2** < **L3** and **1** < **2** < **3** (Table 3). The quenching rates of **1**−**3** are significantly higher than those of the prototypical $ReBr(bpy)(CO)_3$/TEOA/DMF system ($k_q = 3.4 \times 10^7$ M^{-1} s^{-1}[135]), of cationic $[Re(bpy)(CO)_3(4\text{-X-py})]^+$ complexes ($k_q = 2.7 \times 10^8$ to 6.6×10^8 M^{-1} s^{-1}[142]) and of a cationic C_3-bridged $[(4,4'\text{-Mebpy})_2Ru{\sim}ReCl(4,4'\text{-Me}_2bpy)(CO)_3]^{2+}$ complex/BNAH ($k_q = 1.4 \times 10^8$ M^{-1} s^{-1}; BNAH = 1-benzyl-1,4-dihydronicotinamide).[52] For **2** and **3** (and its $[BPh_4]^-$ salt **3***, Table 3), the rates practically correspond to the diffusion limit ($k = 1.9 \times 10^{10}$ M^{-1} s^{-1}, 298 K, CH_3CN), supporting an efficient photoinduced electron transfer to the excited complex.

Table 3. Excited State Redox Potentials (E/V vs. Fc/Fc^+) of L1−L3 and 1−3 in $CH_3CN/[n\text{Bu}_4N][PF_6]$ at Room Temperature, Stern−Volmer Constants K_{SV} (M^{-1}), Estimated Bimolecular Quenching Rate Constants k_q (M^{-1} s^{-1}), and Quenching Fractions η_q by 0.1 M TEOA

	$Ru^{II/III}$[a]	$[ligand]^{0/-}$[b]	K_{SV}	k_q[c]	η_q[d]
L1	−1.23	0.38	1.0	3.9×10^7	0.09
L2	−1.00	0.42	9.9	3.8×10^8	0.50
L3	−0.98	0.33	32	1.2×10^9	0.76
1	−1.20	0.42	97	3.7×10^9	0.91
2	−0.99	0.42	691	2.6×10^{10}	0.99
3	−0.98	0.37	929	3.5×10^{10}	0.99
3*			515	1.9×10^{10}	0.98

[a]Estimated from $E_{ox}^* = E_{ox} - E_{00}$, E_{00} from λ_{em}(77 K). [b]$E_{red}^* = E_{red} + E_{00}$, E_{00} from λ_{em}(77 K). [c]$k_q = K_{SV}/\tau$; τ = 21.7 − 33.7 ns.[14−16] [d]Quenching fractions of emission from ^{3}MLCT(Ru) by 0.1 M TEOA in CH_3CN, λ_{exc} = 500 nm according to $\eta_q = 1 - (1/(1+K_{SV} \times [TEOA]))$.

dx.doi.org/10.1021/ic301632y | Inorg. Chem. 2013, 52, 1248−1264

Finally, we attempted to photocatalytically reduce CO_2 with TEOA as a sacrificial reducing agent and **1**−**3** as bimetallic photocatalysts. Irradiating CO_2 saturated solutions of **1**−**3** in the presence of TEOA at 400 nm (^{3}MLCT(Re)) or at 470 nm (^{3}MLCT(Ru)) yielded no CO under our conditions. This observation might be due to the "wrong" site of the localization of the odd electron in the one-electron reduced species $[\mathbf{1}]^-$−$[\mathbf{3}]^-$ (tpy-CO instead of bpy, vide supra), which are thus incompetent to bind and activate CO_2. With **3*** displaying a favorable spin density at the (bpy)Re site in the one-electron reduced species $[\mathbf{3}^*]^-$, CO_2 binding should be possible after chloride loss (vide supra). However, CO formation was not observed either under these conditions (TEOA, 470 nm). We ascribe this failure to the inability of the one-electron reduced species $[\mathbf{3}^*]^-$ to reduce the CO_2 adduct. Indeed, catalytic chemical CO_2 reduction is feasible using **3*** as a catalyst and $CoCp^*_2$ as a competent reductant (for the second reduction), but no CO formation is observed using **3*** and the weak reductant $CoCp_2$ or $CoCp^*_2$ without **3***.

CONCLUSIONS

Versatile cationic metallo ligands **L1**−**L3** based on bis(terpyridine) ruthenium(II) with differently substituted bipyridines attached via amide groups (5-NHCO, 4-CONH, 5-CONH) were prepared. In the solid state, the amide groups of **L2** and **L3** are hydrogen-bonded to $[PF_6]^-$ counterions either directly via NH···F bonds or indirectly via water molecules giving contact ion pairs and solvent-separated ion pairs, respectively. Oxidation to $[\mathbf{L1}]^+$−$[\mathbf{L3}]^+$ takes place at ruthenium (with some tpy-NH_2 contribution for $[\mathbf{L1}]^+$) while the first reduction to $[\mathbf{L1}]^-$−$[\mathbf{L3}]^-$ occurs at the tpy-CO ligand with a small contribution of Ru in all cases. The lowest energy ^{3}MLCT states $^3[\mathbf{L1}]$−$^3[\mathbf{L3}]$ are best described as charge transfer states involving ruthenium and the tpy-CO ligand (^{3}MLCT(Ru)).

The bpy site of **L1**−**L3** coordinates to $Re^ICl(CO)_3$ fragments constituting the second metallo chromphore in **1**−**3**. According to optical data and redox potentials only a weak communication is established in the ground state. The lowest ^{3}MLCT state $^3[\mathbf{1}]$−$^3[\mathbf{3}]$ is localized at the (tpy-CO)Ru site in all cases similar to $^3[\mathbf{L1}]$−$^3[\mathbf{L3}]$. Energy transfer between electronically excited states (^{3}MLCT(Re) → ^{3}MLCT(Ru)) is observed by emission spectroscopy at room temperature and at 77 K. The $Ru^{II/III}$ oxidation to $[\mathbf{1}]^+$−$[\mathbf{3}]^+$ is essentially unaffected by the additional Re^I moiety, while the site of the first reduction subtly depends on the amide orientation and the counterion. The odd electron is localized at the bridging tpy-CO unit in $[\mathbf{1}]^-$ while the bpy-CO ligand competes as the preferred site in $[\mathbf{2}]^-$ and $[\mathbf{3}]^-$. With a hydrogen-bonding $[PF_6]^-$ counterion at the amide group ($[\mathbf{3}]^-$) the spin density is located at the terminal tpy-CO unit, while with a noncoordinating $[BPh_4]^-$ ($[\mathbf{3}^*]^-$) the spin density is shifted to the bridging bpy-CO unit. A second reduction of **1**−**3** leads to a loss of the rhenium-bound chloride ion and subsequent dimerization via a Re−Re bond. Using triethanolamine as a reducing agent, the excited states $^3[\mathbf{1}]$−$^3[\mathbf{3}]$/$^3[\mathbf{3}^*]$ are efficiently quenched. However, photocatalytic reduction of carbon dioxide using **1**−**3**/TEOA was unsuccessful due to the wrong site of electron localization in the one-electron reduced species $[\mathbf{1}]^-$−$[\mathbf{3}]^-$. The potential photocatalyst **3*** featuring spin-density at the bpy-CO unit in the one-electron-reduced species $[\mathbf{3}^*]^-$ is able to catalytically reduce CO_2 with the strong chemical reductant $CoCp_2^*$ needed for the second reduction step. However, the photolytically formed one-electron reduced species $[\mathbf{3}^*]^-$ itself is incompetent to reduce the CO_2 adduct in the second reduction step, preventing a photocatalytic cycle in this case.

The complexity of the presented systems (anion/solvent/substrate coordination to amide, excited state energy transfer, redox processes at different sites, redox-induced ligand loss from Re) is certainly still far from that of biological systems. Considering the size of the presented systems as compared to multimetallo enzymes, however, amide-linked bimetallic complexes **1**−**3** display a considerable multisite reactivity. We envisage further bimetallic complexes based on **L1**−**L3** for advanced light and redox induced processes, possibly controlled and regulated by coordination of counterions to the connecting amide unit ("alloelectronic control").

ASSOCIATED CONTENT

Supporting Information

Table of geometrical parameters of hydrogen bonds in **L2** and in **L3**·HPF_6 and thermal ellipsoid plots; DFT (B3LYP, LANL2DZ, IEFPCM) optimized geometries of **L1**−**L3**; Kohn−Sham molecular orbitals of **L1**−**L3**; spin densities of $[\mathbf{L1}]^+$−$[\mathbf{L3}]^+$, $[\mathbf{L1}]^-$ − $[\mathbf{L3}]^-$, and $^3[\mathbf{L1}]$ − $^3[\mathbf{L3}]$; X-band EPR spectrum of $[\mathbf{L2}]^-$ and simulation; X-band EPR spectra of $[\mathbf{B}]^+$, $[\mathbf{L1}]^+$, and $[\mathbf{1}]^+$ and simulations; electronic spectra of **1** during oxidation; electronic spectra of **1**−**3** during reduction; IR spectra of **1**−**3** and **3*** after one-electron reduction and after excess $CoCp^*_2$; X-band EPR spectra of $[\mathbf{3}]^-$ and $[\mathbf{3}^*]^-$ and simulation, emission spectra of **3** and **3*** at 300 K in deaerated CH_3CN; excitation emission matrices of **L1**−**L3** and **1**−**3** in deaerated CH_3CN at room temperature; Kohn−Sham molecular orbitals of **1**−**3**; Stern−Volmer plots of **L1**−**L3**; Stern−Volmer plots of **1**−**3** and **3***; Cartesian coordinates of DFT optimized geometries; and X-ray crystallographic data for **L2**·2.4CH_3CN and **L3**·HPF_6·$2H_2O$ in CIF format. This material is available free of charge via the Internet at http://pubs.acs.org/.

AUTHOR INFORMATION

Corresponding Author

*Fax: +49-6131-39-27277. E-mail: katja.heinze@uni-mainz.de.

Notes

The authors declare no competing financial interest.

ACKNOWLEDGMENTS

We thank the Deutsche Forschungsgemeinschaft for supporting our work (He 2778/5-2). We are grateful to Regine Jung-Pothmann for the X-ray data collection, to Anica Wünsche von Leupoldt for the EPR simulations, to Prof. Dr. Thorsten Hoffmann for access to the gas chromatograph, and to the graduate students Sebastian Resch and Jonathan Rosemann for preparative assistance (all Johannes Gutenberg−University of Mainz).

REFERENCES

(1) Juris, A.; Balzani, V.; Barigelletti, F.; Campagna, S.; Belser, P.; von Zelewsky, A. *Coord. Chem. Rev.* **1988**, *84*, 85−277.

(2) Campagna, S.; Puntoriero, F.; Nastasi, F.; Bergamini, G.; Balzani, V. *Top. Curr. Chem.* **2007**, *280*, 117−214.

(3) Bomben, P. G.; Gordon, T. J.; Schott, E.; Berlinguette, C. P. *Angew. Chem., Int. Ed.* **2011**, *50*, 10682−10685.

(4) Narayanam, J. M. R; Stephenson, C. R. J. *Chem. Soc. Rev.* **2011**, *40*, 102−113.

(5) Kiwi, J.; Grätzel, M. *Nature* **1979**, *281*, 657−658.
(6) Kiwi, J.; Grätzel, M. *J. Am. Chem. Soc.* **1979**, *101*, 7214−7217.
(7) Sala, X.; Romero, I.; Rodriguez, M.; Escriche, L.; Llobet, A. *Angew. Chem., Int. Ed.* **2009**, *48*, 2842−2852.
(8) Ceroni, P.; Bergamini, G.; Balzani, V. *Angew. Chem., Int. Ed.* **2009**, *48*, 8516−8518.
(9) Gong, L.; Mulcahy, S. P.; Harms, K.; Meggers, E. *J. Am. Chem. Soc.* **2009**, *131*, 9602−9603.
(10) Cavazzini, M.; Quici, S.; Scalera, C.; Puntoriero, F.; La Ganga, G.; Campagna, S. *Inorg. Chem.* **2009**, *48*, 8578−8592.
(11) Maestri, M.; Armaroli, N.; Balzani, V.; Constable, E. C.; Cargill Thompson, A. M. W. *Inorg. Chem.* **1995**, *34*, 2759−2767.
(12) Schubert, U. S.; Hofmeier, H.; Newkome, G. R. *Modern Terpyridine Chemistry*; Wiley-VCH: Weinheim, Germany, 2006.
(13) Bolink, H. J.; Cappelli, L.; Coronado, E.; Gaviña, P. *Inorg. Chem.* **2005**, *44*, 5966−5968.
(14) Heinze, K.; Hempel, K.; Beckmann, M. *Eur. J. Inorg. Chem.* **2006**, 2040−2050.
(15) Heinze, K.; Hempel, K.; Tschierlei, S.; Schmitt, M.; Popp, J.; Rau, S. *Eur. J. Inorg. Chem.* **2009**, 3119−3126.
(16) Heinze, K.; Hempel, K. *Chem.—Eur. J.* **2009**, *15*, 1346−1358.
(17) Abrahamsson, M.; Wolpher, H.; Johansson, O.; Larsson, J.; Kritikos, M.; Eriksson, L.; Norrby, P.-O.; Bergquist, J.; Sun, L.; Åkermark, B.; Hammarström, L. *Inorg. Chem.* **2005**, *44*, 3215−3225.
(18) Abrahamsson, M.; Jäger, M.; Österman, T.; Eriksson, L.; Persson, P.; Becker, H.-C.; Johansson, O.; Hammarström, L. *J. Am. Chem. Soc.* **2006**, *128*, 12616−12617.
(19) Abrahamsson, M.; Jäger, M.; Kumar, R. J.; Österman, T.; Persson, P.; Becker, H.-C.; Johansson, O.; Hammarström, L. *J. Am. Chem. Soc.* **2008**, *130*, 15533−15542.
(20) Jäger, M.; Kumar, R. J.; Görls, H.; Bergquist, J.; Johansson, O. *Inorg. Chem.* **2009**, *48*, 3228−3238.
(21) Kumar, R. J.; Karlsson, S.; Streich, D.; Rolandini Jensen, A.; Jäger, M.; Becker, H.-C.; Bergquist, J.; Johansson, O.; Hammarström, L. *Chem.—Eur. J.* **2010**, *16*, 2830−2842.
(22) Jäger, M.; Smeigh, A.; Lombeck, F.; Görls, H.; Collin, J.-P.; Sauvage, J.-P.; Hammarström, L.; Johansson, O. *Inorg. Chem.* **2010**, *49*, 374−376.
(23) Schramm, F.; Meded, V.; Fliegl, H.; Fink, K.; Fuhr, O.; Qu, Z.; Klopper, W.; Finn, S.; Keyes, T. E.; Ruben, M. *Inorg. Chem.* **2009**, *48*, 5677−5684.
(24) Breivogel, A.; Förster, C.; Heinze, K. *Inorg. Chem.* **2010**, *49*, 7052−7056.
(25) Breivogel, A.; Hempel, K.; Heinze, K. *Inorg. Chim. Acta* **2011**, *374*, 152−162.
(26) (a) Heinze, K.; Beckmann, M.; Hempel, K. *Chem.—Eur. J.* **2008**, *14*, 9468−9480. (b) zur Borg, L.; Domanski, A. L.; Breivogel, A.; Bürger, M.; Berger, R.; Heinze, K.; Zentel, R. *J. Mater. Chem. C* **2013**, DOI :10.1039/C2TC00535B.
(27) Heinze, K.; Wild, U.; Beckmann, M. *Eur. J. Inorg. Chem.* **2007**, 617−623.
(28) Siebler, D.; Förster, C.; Heinze, K. *Dalton Trans.* **2011**, *40*, 3558−3575.
(29) Constable, E. C. *Chem. Commun.* **1997**, 1073−1080.
(30) Serroni, S.; Campagna, S.; Puntoriero, F.; Di Pietro, C.; McClenaghan, N. D.; Loiseau, F. *Chem. Soc. Rev.* **2001**, *30*, 367−375.
(31) Pelleteret, D.; Fletcher, N. C. *Eur. J. Inorg. Chem.* **2008**, 3597−3605.
(32) Worl, L. A.; Duesing, R.; Chen, P.; Ciana, L. D.; Meyer, T. J. *J. Chem. Soc., Dalton Trans.* **1991**, 849−858.
(33) Nahhas, A. E.; Consani, C.; Blanco-Rodríguez, A. M.; Lancaster, K. M.; Braem, O.; Cannizzo, A.; Towrie, M.; Clark, I. P.; Záliš, S.; Chergui, M.; Vlček, A., Jr. *Inorg. Chem.* **2011**, *50*, 2932−2943.
(34) Hawecker, J.; Lehn, J.-M.; Ziessel, R. *J. Chem. Soc., Chem. Commun.* **1983**, 536−538.
(35) Hawecker, J.; Lehn, J.-M.; Ziessel, R. *Helv. Chim. Acta* **1986**, *69*, 1990−2012.
(36) Christensen, P.; Hamnett, A.; Muir, A. V. G.; Timney, J. A. *J. Chem. Soc., Dalton Trans.* **1992**, 1455−1463.
(37) Ishitani, O.; George, M. W.; Ibusuki, T.; Johnson, F. P. A.; Koike, K.; Nozaki, K.; Pac, C.; Turner, J. J.; Westwell, J. R. *Inorg. Chem.* **1994**, *33*, 4712−4717.
(38) Stor, G. J.; Hartl, F.; van Outersterp, J. W. M.; Stufkens, D. J. *Organometallics* **1995**, *14*, 1115−1131.
(39) Hori, H.; Johnson, F. P. A.; Koike, K.; Ishitani, O.; Ibusuki, T. *J. Photochem. Photobiol., A* **1996**, *96*, 171−174.
(40) Johnson, F. P. A.; George, M. W.; Hartl, F.; Turner, J. J. *Organometallics* **1996**, *15*, 3374−3387.
(41) Koike, K.; Hori, H.; Ishizuka, M.; Westwell, J. R.; Takeuchi, K.; Ibusuki, T.; Enjouji, K.; Konno, H.; Sakamoto, K.; Ishitani, O. *Organometallics* **1997**, *16*, 5724−5729.
(42) Horia, H.; Ishiharaa, J.; Koikea, K.; Takeuchia, K.; Ibusukia, T.; Ishitani, O. *J. Photochem. Photobiol., A* **1999**, *120*, 119−124.
(43) Hayashi, Y.; Kita, S.; Brunschwig, B. S.; Fujita, E. *J. Am. Chem. Soc.* **2003**, *125*, 11976−11987.
(44) Kurz, P.; Probst, B.; Spingler, B.; Alberto, R. *Eur. J. Inorg. Chem.* **2006**, 2966−2974.
(45) Takeda, H.; Koike, K.; Inoue, H.; Ishitani, O. *J. Am. Chem. Soc.* **2008**, *130*, 2023−2031.
(46) Morris, A. J.; Meyer, G. J.; Fujita, E. *Acc. Chem. Res.* **2009**, *42*, 1983−1994.
(47) Doherty, M. D.; Grills, D. C.; Fujita, E. *Inorg.Chem.* **2009**, *48*, 1796−1798.
(48) Smieja, J. M.; Kubiak, C. P. *Inorg. Chem.* **2010**, *49*, 9283−2989.
(49) Kumar, B.; Smieja, J. M.; Kubiak, C. P. *J. Phys. Chem. C* **2010**, *114*, 14220−14223.
(50) Bruckmeier, C.; Lehenmeier, M. W.; Reithmeier, R.; Rieger, B.; Herranz, J.; Kavakli, C. *Dalton Trans.* **2012**, *41*, 5026−5037.
(51) Gholamkhass, B.; Mametsuka, H.; Koike, K.; Tanabe, T.; Furue, M.; Ishitani, O. *Inorg. Chem.* **2005**, *44*, 2326−2336.
(52) Sato, S.; Koike, K.; Inoue, H.; Ishitani, O. *Photochem. Photobiol. Sci.* **2007**, *6*, 454−461.
(53) Bian, Z.-Y.; Sumi, K.; Furue, M.; Sato, S.; Koike, K.; Ishitani, O. *Inorg. Chem.* **2008**, *47*, 10801−10803.
(54) Takedaa, H.; Ishitani, O. *Coord. Chem. Rev.* **2010**, *254*, 346−354.
(55) Bian, Z.-Y.; Chi, S.-M.; Li, L.; Fu, W. *Dalton Trans.* **2010**, *39*, 7884−7887.
(56) Yokoi, N.; Miura, Y.; Huang, C.-Y.; Takatani, N.; Inaba, H.; Koshiyama, T.; Kanamaru, S.; Arisaka, F.; Watanabe, Y.; Kitagawa, S.; Ueno, T. *Chem. Commun.* **2011**, *47*, 2074−2076.
(57) Tamaki, Y.; Watanabe, K.; Koike, K.; Inoue, H.; Morimoto, T.; Ishitani, O. *Faraday Discuss.* **2012**, *155*, 115−127.
(58) Bian, Z.-Y.; Wang, H.; Fu, W.-F.; Li, L.; Ding, A.-Z. *Polyhedron* **2012**, *32*, 78−85.
(59) Shen, Y.; Sullivan, B. P. *J. Chem. Educ.* **1997**, *74*, 685−689.
(60) Curiel, D.; Beer, P. D. *Chem. Commun.* **2005**, 1909−1911.
(61) Higgins, B.; DeGraff, B. A. *Inorg. Chem.* **2005**, *44*, 6662−6669.
(62) Cattaneo, M.; Fagalde, F.; Katz, N. E. *Inorg. Chem.* **2006**, *45*, 6884−6891.
(63) Pelleteret, D.; Fletcher, N. C.; Doherty, A. P. *Inorg. Chem.* **2007**, *46*, 4386−4388.
(64) Brückmann, N. E.; Kögel, S.; Hamacher, A.; Kassack, M. U.; Kunz, P. C. *Eur. J. Inorg. Chem.* **2010**, 5063−5068.
(65) Lo, K. K.-W.; Zhang, K. Y.; Li, S. P.-Y. *Eur. J. Inorg. Chem.* **2011**, 3551−3568.
(66) Heinze, K.; Siebler, D. *Z. Anorg. Allg. Chem.* **2007**, *633*, 2223−2233.
(67) Siebler, D.; Linseis, M.; Gasi, T.; Carrella, L. M.; Winter, R. F.; Förster, C.; Heinze, K. *Chem.—Eur. J.* **2011**, *17*, 4540−4551.
(68) Molina, P.; Tárraga, A.; Caballero, A. *Eur. J. Inorg. Chem.* **2008**, 3401−3417.
(69) Beer, P. D.; Gale, P. A. *Angew. Chem., Int. Ed.* **2001**, *40*, 486−516.
(70) Gale, P. A.; García-Carrido, S. E.; Garric, J. *Chem. Soc. Rev.* **2008**, *37*, 151−190.
(71) Caltagirone, C.; Gale, P. A. *Chem. Soc. Rev.* **2009**, *38*, 520−563.
(72) Heinze, K.; Schlenker, M. *Eur. J. Inorg. Chem.* **2005**, 66−71.

(73) Siebler, D.; Förster, C.; Heinze, K. *Eur. J. Inorg. Chem.* **2010**, 523−527.
(74) Siebler, D.; Förster, C.; Gasi, T.; Heinze, K. *Organometallics* **2011**, *30*, 313−327.
(75) (a) Ozawa, H.; Haga, M.; Sakai, K. *J. Am. Chem. Soc.* **2006**, *128*, 4926−4927. (b) Ozawa, H.; Sakai, K. *Chem. Commun.* **2011**, *47*, 2227−2242.
(76) Ozawa, H.; Sakai, K. *Chem. Lett.* **2007**, *36*, 920−921.
(77) Ashford, D. L.; Stewart, D. J.; Glasson, C. R.; Binstead, R. A.; Harrison, D. P.; Norris, M. R.; Concepcion, J. J.; Fang, Z.; Templeton, J. L.; Meyer, T. J. *Inorg. Chem.* **2012**, *51*, 6428−6430.
(78) Caspar, J. V.; Meyer, T. J. *J. Am. Chem. Soc.* **1983**, *105*, 5583−5590.
(79) Suzuki, K.; Kobayashi, A.; Kaneko, S.; Takehira, K.; Yoshihara, T.; Ishida, H.; Shiina, Y.; Oishic, S.; Tobita, S. *Phys. Chem. Chem. Phys.* **2009**, *11*, 9850−9860.
(80) Stoll, S.; Schweiger, A. *J. Magn. Reson.* **2006**, *178*, 42−55.
(81) SMART Data Collection and SAINT-Plus Data Processing Software for the SMART System (various versions): Bruker Analytical X-Ray Instruments, Inc.: Madison, WI, 2000.
(82) Blessing, R. H. *Acta Crystallogr.* **1995**, *A51*, 33−38.
(83) Sheldrick, G. M. *SHELXTL*, version 5.1; Bruker AXS: Madison, WI, 1998.
(84) Sheldrick, G. M. *SHELXL-97*; University of Göttingen: Göttingen, Germany, 1997.
(85) Frisch, M. J.; Trucks, G. W.; Schlegel, H. B.; Scuseria, G. E.; Robb, M. A.; Cheeseman, J. R.; Scalmani, G.; Barone, V.; Mennucci, B.; Petersson, G. A.; Nakatsuji, H.; Caricato, M.; Li, X.; Hratchian, H. P.; Izmaylov, A. F.; Bloino, J.; Zheng, G.; Sonnenberg, J. L.; Hada, M.; Ehara, M.; Toyota, K.; Fukuda, R.; Hasegawa, J.; Ishida, M.; Nakajima, T.; Honda, Y.; Kitao, O.; Nakai, H.; Vreven, T.; Montgomery, J. A., Jr.; Peralta, J. E.; Ogliaro, F.; Bearpark, M.; Heyd, J. J.; Brothers, E.; Kudin, K. N.; Staroverov, V. N.; Kobayashi, R.; Normand, J.; Raghavachari, K.; Rendell, A.; Burant, J. C.; Iyengar, S. S.; Tomasi, J.; Cossi, M.; Rega, N.; Millam, J. M.; Klene, M.; Knox, J. E.; Cross, J. B.; Bakken, V.; Adamo, C.; Jaramillo, J.; Gomperts, R.; Stratmann, R. E.; Yazyev, O.; Austin, A. J.; Cammi, R.; Pomelli, C.; Ochterski, J. W.; Martin, R. L.; Morokuma, K.; Zakrzewski, V. G.; Voth, G. A.; Salvador, P.; Dannenberg, J. J.; Dapprich, S. Daniels, A. D.; Farkas, O.; Foresman, J. B.; Ortiz, J. V.; Cioslowski, J.; Fox, D. J. *Gaussian 09*, Revision A.02; Gaussian, Inc.: Wallingford, CT, 2009.
(86) Zhang, B.; Breslow, R. *J. Am. Chem. Soc.* **1997**, *119*, 1676−1681.
(87) Lützen, A.; Hapke, M. *Eur. J. Org. Chem.* **2002**, 2292−2297.
(88) Smith, A. P.; Savage, S. A.; Love, J. C.; Fraser, C. L. *Org. Synth.* **2004**, *10*, 517.
(89) Beyermann, M.; Bienert, M.; Niedrich, H. *J. Org. Chem.* **1990**, *55*, 721−728.
(90) Vass, E.; Hollósi, M.; Besson, F.; Buchet, R. *Chem. Rev.* **2003**, *103*, 1917−1954.
(91) Robinson, G. W.; Frosch, R. P. *J. Chem. Phys.* **1962**, *37*, 1962−1973.
(92) Robinson, G. W.; Frosch, R. P. *J. Chem. Phys.* **1963**, *38*, 1187−1203.
(93) Van Houten, J.; Watts, R. J. *J. Am. Chem. Soc.* **1975**, *97*, 3843−3844.
(94) McClanahan, S. F.; Kincaid, J. R. *J. Am. Chem. Soc.* **1986**, *108*, 3840−3841.
(95) Szemes, F.; Hesek, D.; Chen, Z.; Dent, S. W.; Drew, M. G. B.; Goulden, A. J.; Graydon, A. R.; Grieve, A.; Mortimer, R. J.; Wear, T.; Weightman, J. S.; Beer, P. D. *Inorg. Chem.* **1996**, *35*, 5868−5879.
(96) Connelly, N. G.; Geiger, W. E. *Chem. Rev.* **1996**, *96*, 877−910.
(97) Berger, R. M.; McMillin, D. R. *Inorg. Chem.* **1988**, *27*, 4245−4249.
(98) Morris, D. E.; Hanck, K. W.; DeArmond, M. K. *J. Electroanal. Chem.* **1983**, *149*, 115−130.
(99) Sondaz, E.; Gourdon, A.; Launay, J.-P.; Bonvoisin, J. *Inorg. Chim. Acta* **2001**, *316*, 79−88.
(100) Yao, C.-J.; Zhong, Y.-W.; Yao, J. *J. Am. Chem. Soc.* **2011**, *133*, 15697−15706.
(101) Kämper, S.; Paretzki, A.; Fiedler, J.; Záliš, S.; Kaim, W. *Inorg. Chem.* **2012**, *51*, 2097−2104.
(102) Hinderberger, D.; Schmelz, O.; Rehahn, M.; Jeschke, G. *Angew. Chem., Int. Ed.* **2004**, *43*, 4616−4621.
(103) Furue, M.; Naiki, M.; Kanematsu, Y.; Kushida, T.; Kamachia, M. *Coord. Chem. Rev.* **1991**, *111*, 221−226.
(104) Van Wallendael, S.; Perkovic, M. W.; Rillema, D. P. *Inorg. Chim. Acta* **1993**, *213*, 253−260.
(105) Bardwell, D. A.; Barigelletti, F.; Cleary, R. L.; Flamigni, L.; Guardigli, M.; Jeffery, J. C.; Ward, M. D. *Inorg. Chem.* **1995**, *34*, 2438−2446.
(106) Cleary, R. L.; Byrom, K. J.; Bardwell, D. A.; Jeffery, J. C.; Ward, M. D.; Calogero, G.; Armaroli, N.; Flamigni, L.; Barigelletti, F. *Inorg. Chem.* **1997**, *36*, 2601−2609.
(107) Lazarides, T.; Barbieri, A.; Sabatini, C.; Barigelletti, F.; Adams, H.; Ward, M. D. *Inorg. Chim. Acta* **2007**, *360*, 814−824.
(108) Kaim, W.; Kohlmann, S. *Chem. Phys. Lett.* **1987**, *139*, 365−369.
(109) Andréa, R. R.; de Lange, W. G. J.; van der Graaf, T.; Rijkhoff, M.; Stufkens, D. J.; Oskam, A. *Organometallics* **1988**, *7*, 1100−1106.
(110) Scheiring, T.; Klein, A.; Kaim, W. *J. Chem. Soc., Perkin Trans. 2* **1997**, 2569−2571.